

bradscholars

Performance of thermally enhanced geo-energy piles and walls

Item Type	Article
Authors	Elkezza, O.;Mohamed, Mostafa H.A.;Khan, Amir
Citation	Elkezza O, Mohamed M and Khan A (2022) Performance of thermally enhanced geo-energy piles and walls. Geothermics. 98: 102274.
DOI	https://doi.org/10.1016/j.geothermics.2021.102274
Rights	© 2021 Elsevier Ltd. All rights reserved. Reproduced in accordance with the publisher's self-archiving policy. This manuscript version is made available under the CC-BY-NC-ND 4.0 license.
Download date	2025-06-12 10:24:17
Link to Item	http://hdl.handle.net/10454/18799

1 **Performance of thermally enhanced geo-energy piles and walls**

2 Omar Elkezza^a, Mostafa Mohamed^b, Amir Khan^c

3 ^a *PhD research student, Civil and Structural Engineering Department, Faculty of Engineering and*
4 *Informatics, University of Bradford, Bradford, West Yorkshire, BD7 1DP, UK.*

5
6 ^b *Associate Professor, Civil and Structural Engineering Department, Faculty of Engineering and*
7 *Informatics, University of Bradford, Bradford, West Yorkshire, BD7 1DP, UK.*

8 M.h.a.mohamed@bradford.ac.uk

9
10 ^c *Assistant Professor, Civil and Structural Engineering Department, Faculty of Engineering and*
11 *Informatics, University of Bradford, Bradford, West Yorkshire, BD7 1DP, UK.*

12
13 ***Corresponding author:**

14 Dr Mostafa Mohamed

15 Email: M.h.a.mohamed@bradford.ac.uk

16 Phone: +44(0) 1274 233856

17 Fax: +44(0) 1274 2341111

18
19
20
21
22
23
24
25
26
27
28
29
30
31
32
33
34
35
36
37
38 Re-submission
39 09 SEP 2021
40

1 List of nomenclature

2

\dot{m}	Mass flow rate ($\text{kg}\cdot\text{s}^{-1}$)
ΔT	the temperature drop/ difference ($^{\circ}\text{C}$)
A	Cross sectional area (m^2)
C-S-H	Calcium silicate hydrate
C_p	Thermal capacity ($\text{J}\cdot\text{kg}^{-1}\cdot\text{K}^{-1}$)
CTE	Coefficient of thermal expansion
GEP	Geo energy pile
GEW	Geo energy wall
GSHP	Ground source heat pump
HE	Heat exchange
HP	Heat pump
K	Thermal conductivity ($\text{W}/\text{m}\cdot\text{K}$)
L	Specimen thickness (m)
Q	rate of heat transfer (W) or ($\text{J}\cdot\text{s}^{-1}$)
q	the thermal energy dissipated into the ground (W) or ($\text{J}\cdot\text{s}^{-1}$)
T_{in}	Inlet temperature ($^{\circ}\text{C}$)
T_{out}	Outlet temperature ($^{\circ}\text{C}$)
XRD	x-ray diffraction
LDPE	Low density polyethylene
HDPE	High density polyethylene

1 **Performance of thermally enhanced geo-energy piles and walls**

2 Omar Elkezza, Mostafa Mohamed, Amir Khan

3 **Abstract:**

4 This study aims to evaluate the impacts of using thermally enhanced concrete on the thermal
5 performance of geo-energy structures and interaction between the thermo-active-structures and
6 adjacent dry and partly saturated soils. Experiments using a fully instrumented testing rig were carried
7 out on prototypes of energy pile and diaphragm wall made from normal concrete and thermally
8 enhanced concrete by the addition of graphTHERM powder. Results illustrated that adding 36 % of
9 graphTHERM powder to the concrete by weight of cement was found to double the thermal
10 conductivity of concrete and improve the stiffness by 15 % without detrimental effects on the
11 compressive strength. The heat transfer efficiency of energy pile and energy diaphragm wall made
12 from thermally enhanced concrete was significantly improved by 50 % and 66 % respectively, in
13 comparison with the efficiency of the same type of energy structure that was made from a typical
14 normal concrete.

15 **Keywords:** Thermally enhanced concrete, energy pile efficiency, energy diaphragm wall, thermal
16 conductivity of concrete.

17
18
19

1 **1. Introduction**

2 Climate change is one of the critical issues that could negatively impact the environmental, economic
3 and society sustainability of nations across the world if it is not tackled urgently and adequately. More
4 than 160 million buildings across Europe consume over 40 % of the total energy usage which is
5 predominantly coming from burning fossil fuels used for heating, ventilation and air conditioning
6 (Thomas and Rees, 2009). Burning fossil fuels is the most common method for generating energy.
7 Nevertheless, fossil fuels are a depleting source of energy and contribute significantly to elevating
8 carbon emission and greenhouse effect. Widespread use of renewable energy sources is, therefore,
9 essential for the UK and Europe to meet their carbon emission and neutralisation targets and in
10 particular to meet its net zero carbon target.

11 In recent years, the utilisation of shallow geothermal energy for heating of buildings has spread rapidly
12 in Europe and around the world as a viable renewable energy source. The emerging technology, which
13 is known for using such energy, is a Ground Source Heat Pump (GSHP) system. A closed GSHP system
14 is fundamentally made of two components, namely a Heat Pump (HP) and a Heat Exchanger (HE). A
15 HP circulates a coolant fluid in the HE e.g. in pipes that are laid either horizontally or vertically into
16 ground to either extract heat from or reject heat into the ground (Kovačević et al., 2012). Due to the
17 high cost of vertical drilling and the need for a large ground area for placing horizontal HE (loops), the
18 HE pipes are recently being installed within the foundation elements of the structures and buried
19 infrastructures. These structures are currently known as geo-energy structures e.g. energy piles,
20 energy diaphragm walls and tunnel energy lining (Suryatriyastuti et al., 2012). Geo-energy structures
21 are considered interesting and promising tools to tackle the continuous surge in energy demands for
22 heating and cooling of buildings (Brandl, 2006; Laloui and Di Donna, 2013), and could provide a
23 sustainable source of energy for buildings. As a result, the use of Geo-Energy Piles (GEPs) has seen a
24 rapid increase around the world, providing green energy source for many buildings in Europe, Canada,
25 China and Japan (Thomas and Rees, 2009). The heat transfer characteristics of the energy piles have
26 been covered in many studies (Faizal et al., 2016; Cecinato and Loveridge, 2015).

1 Critical analysis of heat transfer mechanisms in geothermal energy piles has demonstrated that there
2 are four key factors affecting the thermal performance of geothermal energy piles which are: i.
3 geometrical optimisation, ii. introduction of a Nanofluid as a coolant/circulating fluid, iii. pipe
4 materials and iv. concrete heat transfer enhancement (Faizal et al., 2016). Geometrical optimisation
5 mainly focuses on the pile dimensions [depth, diameter, concrete cover, etc.] as well as the pipe
6 configuration [number of pipes and pipe arrangements]. Kwag and Krarti (2013) numerically
7 demonstrated that increasing the pile length led to an increase in the heat exchange rate. It was also
8 revealed that when the distance between U-tube loops or shanks space was increased, the extracted
9 and dissipated energy was considerably enhanced. Similarly, Kaltreider et al. (2015) showed that the
10 heat transfer was remarkably higher when larger tube shanks were used. It was also noted that
11 enlarging the pile diameter resulted in a lower concrete thermal resistance (R_{concrete}) for a single U-
12 tube configuration (Loveridge and Powrie, 2014). The double U-shaped pipes were found to produce
13 a better thermal performance than a single U-tube (Li et al., 2014 and Gashti et al., 2014). Increasing
14 the number of pipes inside the energy piles was found to provide an enhanced mechanism to extract
15 more heat from the ground. Jalaluddin et al. (2011) indicated that enhanced coaxial heat exchanger
16 tubes gave an improved heat transfer with the surrounding ground. In other words, increasing the
17 length of the HE pipes inside the foundation elements of the structure increased the extracted heat.
18 Zarrella et al. (2013) pointed out that the helical shaped HE also led to an improvement in the thermal
19 performance and was considered to provide more heat transfer than U-tube shaped HE due to
20 providing higher heat transfer area than the conventional U-tube HE. The geometrical parameters of
21 GEPs were largely governed by the imposed mechanical load of the superstructure rather than the
22 building energy demand. Nevertheless, to enhance the thermal performance, an increase in the pile
23 length and/or pile diameter might be necessary, hence a coupled mechanical and thermal assessment
24 of the GEPs is required to optimise the use of the sub-structural elements of the structures. Lyu et al.
25 (2020)'s proposed a novel heat exchanger configuration for a geo-energy pile, which called a deeply
26 penetrating 1-U-shaped configuration and compared its heat transfer performance with a traditional

1 1-U-shaped and 1-W-shaped configuration. It was revealed that the proposed deeply penetrating 1-
2 U-shaped HE provided superior improvement on the total heat transfer rate giving an increase of 122
3 % when compared with the traditional 1-U-shaped configuration [a single U-tube shaped] and of 55%
4 when compared with 1-W-shaped [a single W-tube shaped] configuration. An optimisation exercise
5 of double-U-tube borehole heat exchanger (BHE) was carried out using the Taguchi Method to rank
6 the most influential parameters on the extracted and rejected heat (Kumar and Murugesan, 2020).
7 Eight parameters were studied including borehole temperature, inlet temperature, borehole radius,
8 half centre distance, grout thermal conductivity, soil thermal conductivity and mass flow rate. The
9 optimization exercise indicated that during heat rejection and extraction (cooling and heating), the
10 inlet temperature and borehole temperature are found to be the most influential parameters on the
11 heat transfer rate, followed by the mass flow rate, centre distance and thermal conductivity of the
12 grouting material. BHE tube radius did not influence the heat transfer rate for cooling mode. In heating
13 mode, the thermal conductivity of soil was found to be the less influential parameter on the heat
14 transfer rate.

15 Several studies examined the effect of mixing nanoscale particles with the circulating fluid to enhance
16 its thermal properties. It was proven that a significant increase in thermal properties of fluid occurred
17 with a small concentration of particles (Das et al., 2006). Ghizatloo et al. (2014)'s tests on
18 Graphene/water fluid with a concentration of 0.050, 0.075 and 0.100 % by weight revealed that the
19 thermal conductivity of the circulating fluid increased when increasing the graphene concentration up
20 to a particular concentration of 0.075 %. For example, measurements taken at 25 °C illustrated that
21 with the addition of 0.05, 0.075 and 0.10 % of graphene by weight in water, the thermal conductivity
22 was increased by 15 %, 29.2 % and 12.6 % respectively. Godson et al. (2014) found that the overall
23 heat transfer coefficient of nanofluids made of silver and water mix was higher than that of water.
24 Furthermore, it was shown that the pressure drop in the case of this nanofluid was higher compared
25 to that observed for the base fluid due to an increase in viscosity, hence more pumping power was

1 needed. Although nanofluids showed a remarkable improvement in thermal conductivity, it did not
2 result in a significant impact on the overall thermal exchange energy (Cecinato and Loveridge, 2015).

3 Due to being the interface element between the circulating fluid and surrounding concrete, pipe
4 material should carefully be selected because of the impacts of its thermal resistivity on controlling
5 the heat transfer, durability and cost effectiveness (Noorollahi et al., 2018). To investigate the effect
6 of pipe material, Selamat et al. (2016) carried out experiments on pipes made of three different types
7 of material: high density polyethylene (HDPE), copper, and a composite (copper and LDPE coating)
8 and with a thermal conductivity of 0.41, 387.6 and 1.19 W/m.K respectively. The heat exchange rate
9 was found to be 206.4, 232.2 and 209.6 W/m respectively. As a result, the copper pipe was revealed
10 to improve the operational efficiency by 16 %. Another investigation (Raymond et al., 2015) using
11 three different types of pipe material: plastic with a thermal conductivity of 0.24 W/m.K, steel with a
12 thermal conductivity of 57 W/m.K and copper with a thermal conductivity of 395 W/m.K, showed that
13 the heat exchange rate (W) for the three pipes was 933.96, 939.89, 939.92 kWh/year respectively.
14 Consequently, the study suggested that the type of the pipe material had no major effect in the system
15 performance which is contradictory to the outcomes of Selamat et al. (2016). Furthermore, by
16 comparing the thermal performance of the steel pipes with that of the HDPE pipes, it was observed
17 that the performance of the steel pipes was higher. This was attributed to the fact that its thermal
18 resistance was about 7 % less than that of the HDPE pipes. In addition, it was reported that due to
19 higher heat exchange rate in the case of steel pipes, a higher soil temperature around the steel pipe
20 was experienced (Cao et al., 2016). Improving the thermal properties of HDPE using different types of
21 conductive fillers such as metallic oxide, non-oxides, graphite and other similar materials was
22 assessed. Dorrian and Mumm (2011) developed a pipe with a higher thermal conductivity of 0.85
23 W/m.K by the addition of a blend of 20 % HDPE, 5 % thermoplastic elastomer and 75 % zinc oxide. The
24 results revealed that using the thermally enhanced pipe material reduced pipe length by almost less
25 than half whilst increasing the extracted heat by 100 %. Ye et al. (2006) experimentally evaluated HDPE

1 filled with expanded and colloid graphite. The thermal conductivity of HDPE pipes increased with the
2 increase in the graphite content whilst expanded graphite led to twice as high thermal conductivity
3 values compared to those measured for HDPE filled with colloid graphite. It is reasonable to highlight
4 that the key considerations for the selection of the pipe material would be dependent on the cost,
5 corrosion resistance, durability and its thermal properties. Hence, HDPE pipes become a sensible
6 choice due to their low cost, corrosion resistance and easy installation.

7 Several studies were carried out aiming at either increasing the compressive strength of concrete or
8 reducing the thermal conductivity of concrete for insulation purposes. Nevertheless, limited
9 investigations were performed to improve the thermal conductivity of concrete (Li et al., 2018). It is,
10 therefore, crucial that the use of novel composite materials is explored to enhance the thermal
11 properties of concrete without losing sight of any potential impacts on the load carrying capacity of
12 structural elements such as the piles. Guo et al. (2010) examined the addition of graphite to improve
13 the thermal conductivity of concrete and pointed out that at room temperature, with an increase in
14 the graphite content, the thermal conductivity of concrete rapidly increased. In another study, a series
15 of graphite concrete specimens were prepared by mixing cement, sand, water, water-reducing agent,
16 and different volumetric content of powdered graphite (0 %, 5 %, 10 %, 15 %, and 25 %). The results
17 indicated that the addition of graphite powder clearly enhanced the thermal conductivity, especially
18 for concrete specimens with graphite contents of more than 15 %. The measured thermal conductivity
19 results were used in a numerical modelling using finite element analysis to investigate the
20 performance of geo-energy pile made of graphite concrete. The results demonstrated the ability of
21 graphite concrete to enhance the heat transfer characteristics of energy piles and showed that a
22 higher graphite content was more beneficial to the heat transfer process. However, the study did not
23 include any field or large-scale experimental measurements (Li et al., 2018). Similar numerical study
24 by Kong et al. (2019) on heat transfer characteristics of graphite concrete was used to thermally
25 enhance energy pile and the results indicated that the heat transfer capacity of the graphite concrete
26 energy pile was higher by 6.5% than that measured on a typical concrete energy pile. Nonetheless,

1 there was no evaluation of the effect of this thermal enhancement on the concrete's compressive
2 strength and there was also a lack of physical measurements of the pile performance.

3 Even though the efficiency of geo-energy piles were studied by several authors e.g. Bao et al. (2019)
4 and Cecinato and Loveridge (2015) limited laboratory investigations were carried out to study the use
5 of diaphragm walls as a geo-energy structure. Kurten et al. (2015) developed a semi-analytical model
6 that was used to evaluate the effects of several factors including ground temperature, inlet
7 temperature, flow rate and thermal conductivity of soil. The model was validated using experimental
8 results and its results showed that the pipe thickness cover, flow rate and inlet temperature are the
9 most important factors which affected extraction of heat using such a structure. However, the results
10 of another numerical study carried out by Di Donna et al. (2016) to evaluate the most influential
11 parameters on the performance of heat exchange using embedded walls revealed that the thermal
12 conductivity of concrete and ground temperature caused significant impacts on the geo-energy wall
13 performance. The behaviour of the geo-energy wall was assessed by a finite element model carried
14 out by Sterpi et al. (2017) to highlight the wall's geotechnical and structural response. The results
15 suggested that the thermally induced effects on the structure were not negligible and could be
16 observed partly in the form of additional displacements and variations of the internal actions. Bourne-
17 Webb et al. (2016) also performed numerical simulations to study the mechanical response of the geo-
18 energy walls under different environment conditions and found that the seasonal changes affected
19 the thermal expansion value for the wall and the soils, hence it should be considered in the design
20 process. Dong et al. (2019) proved through experimental and numerical investigations that a short-
21 term heating of the wall showed a substantial temperature gradient across the wall thickness resulting
22 in a significant stress and strain variation within the wall during the first few hours. Di Donna et al.
23 (2017) published results of the first study on the efficiency of diaphragm walls and found that the
24 concrete thermal conductivity had major effects on the long-term performance of geo-energy
25 diaphragm walls and recommended to carefully design the concrete mix to maximise the thermal
26 conductivity of wall material.

1 In light of the aforementioned critical review of the key parameters affecting the performance of geo-
2 energy structures, it is reasonable to conclude that extensive research studies have been conducted
3 on geo-energy structures with a focus on optimising the geometry of geo-energy structures, heat
4 exchanger coil types and design. However, published work would seem to indicate that less attention
5 has been given to the concrete thermal properties' effect on the performance of the energy piles and
6 diaphragm walls. Consequently, this study reports the outcomes of an experimental investigation
7 conducted using a large-scale fully instrumented laboratory rig for assessing the effects of enhancing
8 the concrete thermal conductivity using graphTHERM addition on the thermal performance of geo-
9 energy structures including piles and walls. The primary objectives of this study are to: i. Optimise the
10 content of graphite to achieve a significantly improved thermal conductivity with minimal/no adverse
11 impact on strength, ii. Assess the heat transfer capacity of geo-energy structures e.g. pile and walls
12 utilising thermally enhanced concrete in dry and partly saturated grounds and iii. Study the thermal
13 expansion and lateral earth pressure on the geo-energy structure.

14 **2. Experimental materials and methods**

15 In order to enable the investigation process of geo-energy structures using thermally enhanced
16 concrete, a fully instrumented testing rig was designed and manufactured to run the heat transfer
17 experiments consisting of three main parts, a testing tank, geo-energy structure and a data acquisition
18 system. Details of the materials used in this experimental programme are demonstrated and discussed
19 hereafter.

20 **2.1 Materials**

21 **2.1.1 Sand**

22 Standard building sand was chosen to simulate the ground soil in this experimental study due to its
23 availability and cost effectiveness. The particle size distribution of the ~~used~~ sand was determined in
24 accordance with BS1377: Part 2 and is shown in Fig. 1. The sand was found to have a mean particle

1 size of 0.24 mm and its characteristic diameters are illustrated in Fig. 1. The coefficients of uniformity
 2 (C_u) and curvature (C_c) were determined and found to be 1.38 and 0.89 respectively. As a result, the
 3 sand used was classified as a poorly graded fine to medium sand. The specific gravity (G_s) of the sand
 4 was determined using the pycnometer method as specified by BS1377:2, 1990 and found to be 2.65.

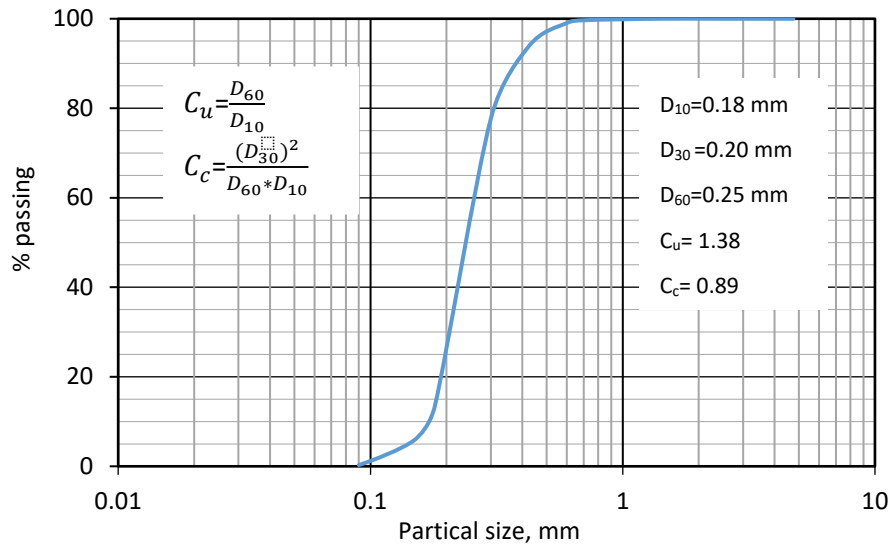


Fig. 1. Particle size distribution of the used sand

13 A standard Proctor Compaction Test was performed according to BS1377-4:1990 in order for the
 14 maximum dry unit weight and optimum moisture content of the sand to be determined. The
 15 compaction test revealed that the maximum dry unit weight and optimum moisture content are 18.15
 16 kN/m^3 and 11 % respectively. In addition, direct shear tests were performed in compliance with BS
 17 1377 part 7 under a range of normal stresses between 70 and 250 kPa to generate data for the normal
 18 stress – shear stress relationships. Based on the acquired data, the friction angle for the sand was
 19 found to be 34.8°.

Table 1: Main properties of the used sand

Parameter	Value	Test Method
Mean particle size, D50 (mm)	0.24	BS.1377:2, 1990

Coefficient of Uniformity, Cu	1.38	
Coefficient of Curvature, Cc	0.89	
Specific gravity, Gs	2.65	BS.1377:2, 1990
Maximum dry unit weight (kN/m ³)	18.15	BS.1377:4, 1990
Optimum water content (%)	11	BS.1377:4, 1990
Angle of friction angle, ϕ (degrees)	34.8	BS.1377:7, 1990
Hydraulic conductivity (m·s ⁻¹)	2.7x10 ⁻⁴	BS.1377:6, 1990

1

2 2.1.2 Graphite powder

3 In this study, a special type of the graphite powder called “graphTHERM” was used to enhance the
4 thermal conductivity of the concrete as it has a less effect on hydration of the concrete besides its
5 high thermal conductivity. The selected graphite powder was developed by Georg H. Luh GmbH and
6 had a high thermal conductivity of more than 100 W/m.K. Based on the data sheet provided by the
7 supplier, graphTHERM was manufactured to be used as a filling material to increase the thermal
8 conductivity without causing significant adverse impacts on the mechanical properties. Table 2
9 presents the main properties of graphTHERM powder as provided by the supplier.

10
11

Table 2: Main properties of graphTHERM

Property	Value
Carbon (%)	Min 99.9
Ash (%)	Min 0.01
Iron (ppm)	100
Tapped density (g/cm ³)	0.85 – 1.05
Thermal conductivity, for cylindrical prepared sample of 1.85 gm.cm ⁻³ and w/c=10 % (W/m.K)	100
Surface area (m ² /g)	6.5-10
D ₁₀ (μm)	10 – 14
D ₅₀ (μm)	18 – 25
D ₉₀ (μm)	30 – 45

19

20

21

1 **2.1.3 Concrete batches**

2 All concrete batches were designed in compliance with the British Standards, BS 8500. Portland
3 limestone cement (CEM II/A-LL 52.5R), manufactured by Hanson UK in accordance with BS EN 197-
4 1:2000 was used in this study. A mix of natural coarse aggregates (NCA) with a maximum particle size
5 of 10 mm and natural fine aggregate (NFA) with a maximum particle size of 5 mm were used in this
6 research. Of note, the NCA particles had predominantly angular shapes. The properties of the coarse
7 and fine aggregates were conformed to the standard requirement limits of BS EN 882. A water/cement
8 (w/c) ratio of 0.45 was chosen to achieve a target compressive strength ranging between 45 - 48 MPa
9 after 28 days. The proportions of the concrete constituents were kept constant for all concrete mixes
10 in this study, the graphite powder was added to the concrete mix as a ratio of the cement by weight.
11 It is imperative to note that the graphite powder was not used as a replacement material in the
12 concrete. The concrete batches were prepared by mixing cement, NFA, NCA, water and graphite
13 powder (graphTHERM). The graphTHERM was added with different weight contents of 0 %, 10 %, 20
14 %, 30 %, 40 % and 50 % by weight of the cement. The materials were mixed in a mechanical pan type
15 mixer for 2-3 min in order for a homogenous mix to be achieved prior to adding the predefined amount
16 of water. The mix was then poured in special cylindrical moulds with an internal diameter of 100 mm
17 and a height of 50 mm as well as in 100 mm cubical moulds. The former was used to create specimens
18 with an appropriate size for measuring ~~the~~ thermal conductivity using a hotplate testing setup,
19 whereas the latter was used to produce standard concrete cubes for assessing the compressive
20 strength of thermally enhanced concrete. Both cylindrical and cubical concrete specimens were cured
21 for 28 days in a water bath followed by 2 days in a drying room with an ambient temperature of 24°C.
22 It was important to dry out the specimens due to the sensitivity of thermal conductivity measurement
23 to moisture content. Afterward, these samples were utilised to determine the optimum graphTHERM
24 content. Subsequently, the optimum percentage of the graphTHERM was used to produce further
25 concrete samples for evaluating the thermal expansion coefficient and concrete stiffness. Of note,
26 concrete prisms with dimensions of 40 x 40 x 160 mm were used to evaluate the concrete thermal

1 expansion coefficient in accordance with TI-B 101 (94), whereas cylindrical concrete samples with a
2 diameter of 100 mm and height of 200 mm were used to determine the concrete stiffness in
3 accordance with EN 1992-1-2, 2004.

4 **2.2 Experimental methods**

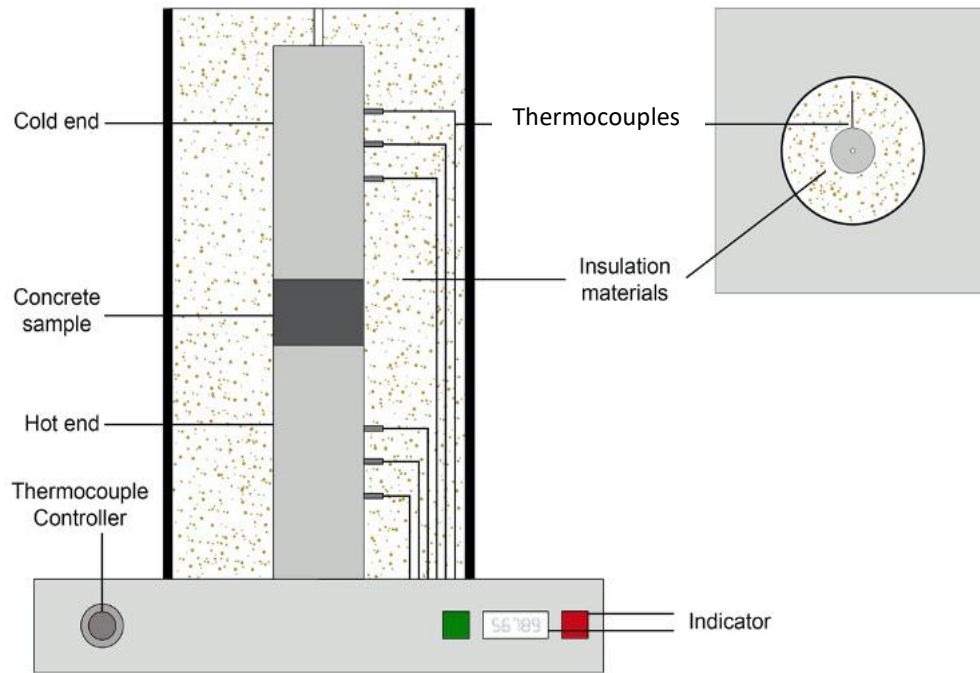
5 **2.2.1 Hot plate setup**

6 Hot plate tests were carried out according to the British Standards - BS EN 12664:2001 to measure the
7 thermal conductivity on cylindrical concrete samples prepared with different percentages of graphite
8 powder by weight of cement. Fig. 2 shows a schematic drawing of the hot plate test. The concrete
9 sample was sandwiched between flat hot and cold plates as shown in Fig. 2. Due to the temperature
10 difference, a thermal gradient was created through the sample. The heat flux, which is defined as the
11 amount of the input heat power passing through the cross-sectional area of the specimen, can be
12 determined from the power input and the cross-sectional area of the specimen. By knowing the
13 temperature drop, heat flux and length of the specimen, Fourier's law of unidirectional heat transfer
14 can be applied to calculate the thermal conductivity (k) in W/m.K as given by Equation 1-

$$k = \frac{Q \cdot L}{A \cdot \Delta T} \quad (1)$$

15 where; Q is the rate of heat transfer (watts), ΔT is the temperature drop ($^{\circ}\text{C}$), L is the specimen
16 thickness (m) and A is the cross-sectional area of the concrete sample (m^2). It is worth noting that the
17 setup was calibrated by measuring the thermal conductivities of sample materials such as wood,
18 aluminium and brass with known thermal conductivity. The results of the calibration exercise showed
19 that the maximum error in the thermal conductivity measurement was found to be 3 %. In addition,
20 measurements were taken on three identical samples and the average value was reported hereafter
21 for each concrete mix.

1



2

Fig. 2. Schematic drawing of the hot plate test experimental setup

3

2.2.2 Heat transfer experiments

4

A Fully instrumented heat transfer testing rig with internal dimensions of 1 m x 1 m x 1 m was designed

5

and manufactured. Figs 3 and 4 show schematic diagrams of the testing rig and configuration of the

6

geo-energy pile and wall respectively. The tank walls are fully insulated to minimise the effect of the

7

ambient air temperature. A drainage system was installed at the base of the tank to uniformly

8

introduce and drain groundwater over the whole cross-section area of the tank. The drainage system

9

included perforated pipes, manifold, gravel bed, a filter sheet and a well. The perforated pipes and

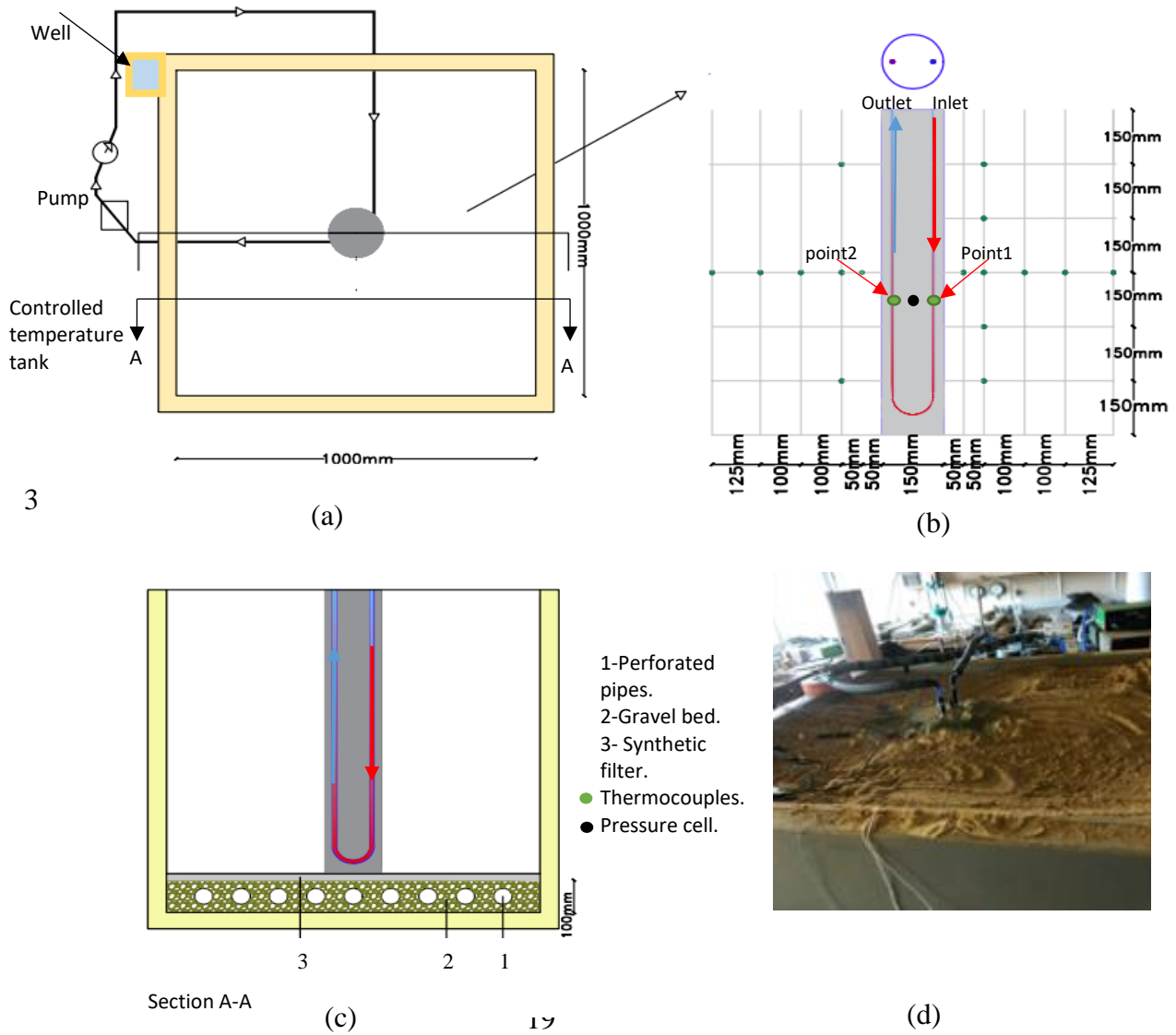
10

manifold were surrounded by a gravel bed that was wrapped by a synthetic filter sheet to prevent

11

washing out of fine sand particles and to avoid blockage of the drainage system. The drainage system

1 (manifold) was connected with an external well to regulate and maintain the water level inside the
 2 tank at pre-determined levels.



20
 21
 22
 23
 24

Fig. 3. Schematic diagram of the experimental rig for energy pile tests; a) Plan view, b) Location of thermocouples, c) Vertical cross section of the testing tank and d) Image of real testing rig.

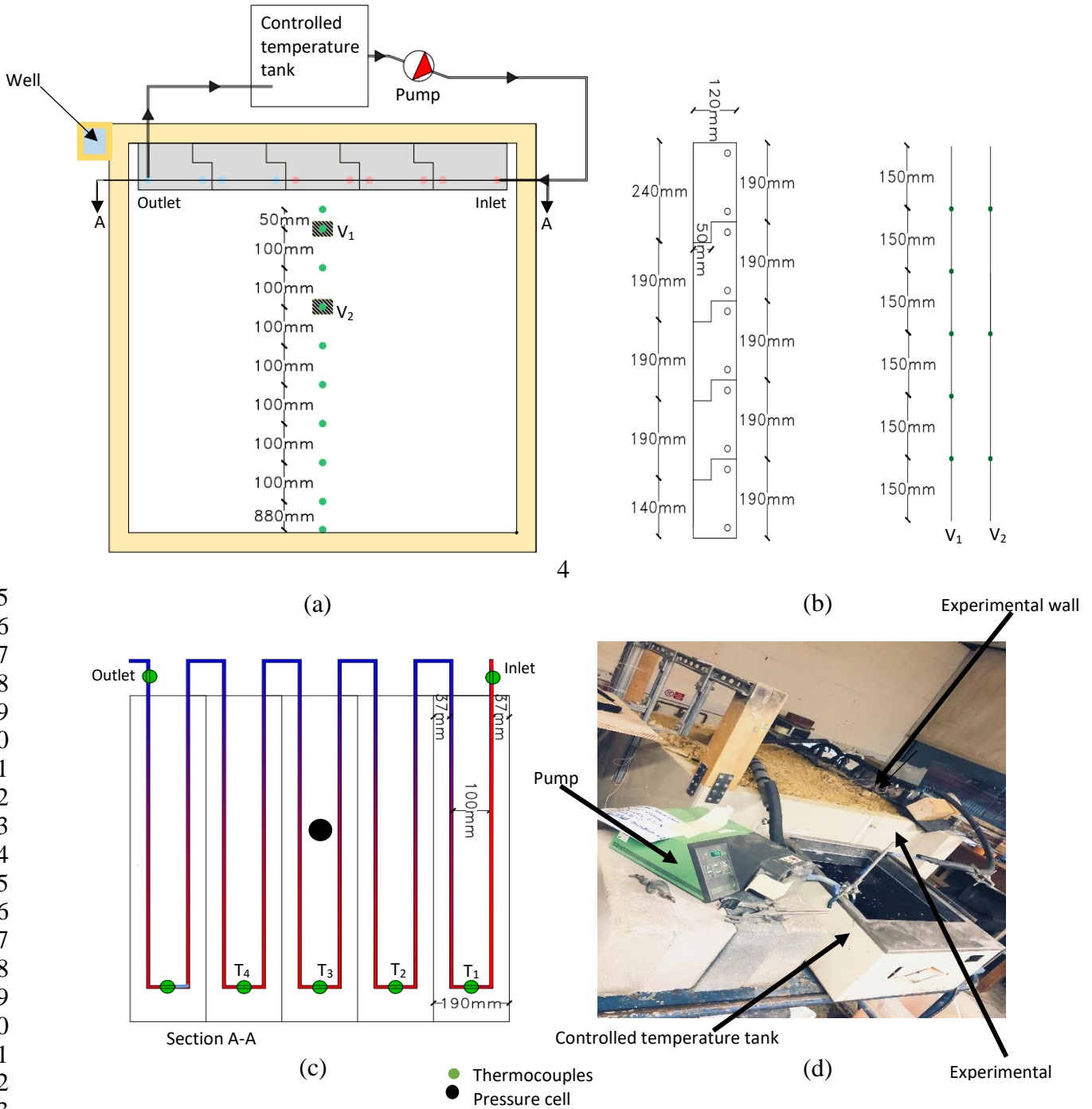


Fig. 4. Schematic diagram for the experimental rig for energy wall test; a) Plan view, b) Dimensions of wall and location of thermocouples, c) Arrangement of heat exchanger and d) Image of real testing rig.

Two different embedded geo-energy structures were examined in this study a concrete energy pile and concrete energy wall. The geo-energy pile was formed with external dimensions of 900 mm in height and 150 mm in diameter. The pile was placed in the centre of the tank and surrounded by sand. A U-shaped heat exchanger [HE] made out of nylon with a total length of 1700mm and outer and inner

1 diameters of 8 mm and 6 mm respectively was embedded symmetrically inside the concrete pile. The
2 concrete energy wall was constructed in 5 segments that were interlocked together to form an
3 embedded wall as shown in Fig. 4b. Each segment of the concrete wall had dimensions of 900 mm in
4 height, 190 mm in width and 120 mm in depth. A nylon U-shaped heat exchanger was embedded in
5 each segment resulting in a total heat exchanger tube length of 9900 mm. In order to fasten the HEs
6 precisely in predefined locations inside the energy piles and walls, metal cages were manufactured
7 and fitted inside the casting mould prior to casting of wet concrete. The centre to centre spacing
8 between the two legs of the U-shaped HE was maintained at 100 mm in the energy piles and walls.
9 After casting the concrete, the energy model structures were cured for 28 days by covering them with
10 wet sheets that were frequently wetted with water to maintain consistent curing conditions.
11 Upon completion of curing period, the geo-energy pile was installed in the centre of the testing tank.
12 To measure the lateral earth pressure on the pile and the wall, an earth pressure cell was installed at
13 a pre-determined location which was at mid-height of pile or the centre point of the wall. The earth
14 pressure cell was placed during the sand filling stage of the tank as shown in Fig. 3b and Fig. 4c. Also,
15 A T-type thermocouple was fastened at mid height of the pile and at the centre point of the wall to
16 measure the temperature of the concrete during the test. The illustrative drawings in Figs 3b, 4a and
17 4b show the location of sensors. The soil temperature was measured at several vertical and horizontal
18 sections. A total of 23 T-type thermocouples were utilised for measuring the vertical and horizontal
19 soil temperature profile, fluid temperature inside the heat exchanger, inlet and outlet temperature
20 and the ambient temperature. A total of 27 T-type thermocouples were required in tests involving
21 the geo-energy wall. All thermocouples were calibrated prior to their use and the accuracy of the
22 measurements were found to be ± 0.25 °C. After the installation of all devices and sand-filling
23 completed, a mix of degradable glycol-water ratio 1 part glycol to 3 parts of water was circulated in
24 the HE that was embedded inside the energy structure with a target temperature of 52 °C. The flow
25 rate of the circulating fluid was controlled using a peristaltic pump at a rate of 67 l/h throughout the
26 tests. In total 6 experiments were carried out including 4 tests on energy piles and 2 tests on energy

1 walls with the fixed and variable parameters demonstrated in Table 3. The first two tests were
 2 conducted on piles that were made from normal concrete and graphite concrete and installed in dry
 3 sand beds as illustrated in Table 3. Two more tests were then performed whilst the sand surrounding
 4 the pile was partly saturated with water by maintaining the water level inside the tank at 500 mm
 5 above the base resulting in a steady hydrostatic water pressure. This is an attempt to simulate a real-
 6 world scenario where geo-energy piles are installed in grounds where groundwater table is stagnant
 7 at a particular level. The final two experiments were carried out on energy walls made of normal and
 8 thermally enhanced concrete materials but installed in a similar ground to the previous two tests in
 9 which sand was partly saturated with water. It should be noted that test coding was developed to
 10 reflect test conditions. For example, a test code W-NW-1 indicated a normal concrete wall installed in
 11 a partly saturated sand whereas test code W-GW-2 indicated an energy wall made out of graphite
 12 concrete in partly saturated sand. Table 3 illustrated the fixed and variable parameters in each
 13 experiment alongside with the test coding. Measurements were taken every 10 second by the data
 14 acquisition system and saved automatically on the computer. An hourly average was then determined
 15 and presented hereafter.

16 Table 3: Fixed and variable parameters for heat transfer experiments

Series	Test coding	Fixed parameters	Variable parameters	Notes
Energy piles 1	D-NP-1	DS, FR = 67 l/h, IT = 52.14 °C	NP	Normal concrete pile installed in dry sand
	D-GP-2	DS, FR = 67 l/h, IT = 52.41 °C	GP	Graphite concrete pile installed in dry sand
	W-NP-3	FR = 67 l/h, PSS, IT = 52.01 °C	NP, WL = 500 mm	Normal concrete pile installed in partly saturated sand
	W-GP-4	FR = 67 l/h, PSS, IT = 52.52 °C	GP, WL = 500 mm	Graphite concrete pile installed in partly saturated sand
Energy 2	W-NW-1	PSS, WL = 500mm FR = 67lh, IT = 53.18 °C	NW	Normal concrete wall installed in partly saturated sand

	W-GW-2	PSS, WL = 500mm FR = 67lh, IT = 52.35 °C	GW	Graphite concrete wall installed in partly saturated sand
--	--------	---	----	---

1 where; DS = Dry Sand, PSS= Partly Saturated Sand, FR = Flow Rate, WL= Water Level and IT = Inlet Temperature,
 2 NP= normal concrete pile, GP= graphTHERM concrete pile, NW= normal concrete wall, GW= graphTHERM
 3 concrete wall.
 4

5 **3. Results and discussion**

6 This section is organised to present and discuss the measurements taken for the thermal conductivity
 7 and thermal heat capacity of sand and the thermal conductivity of concrete before assessing the
 8 behaviour of the geo-energy structures under different conditions. The effect of adding thermal
 9 enhancement material on the concrete thermal conductivity is presented and discussed. These results
 10 are then utilised to support the discussion of the influence of the thermally enhanced concrete on the
 11 performance of geo-energy structures e.g. piles and walls.

12 **3.1 Thermal properties of sand soil**

13 A KD2 Pro thermal analyser device was utilised to measure the thermal properties including thermal
 14 conductivity and thermal capacity of the sand used. Both dry and wet sand samples were prepared
 15 with a constant dry unit weight of 18.15 kN/m³ under a static load. Samples of the wet sand were
 16 prepared with varying water contents of 1 %, 3 %, 5 %, 10 %, 20 % and 30 % and were compacted to
 17 the same dry unit weight. Upon compaction of the sand samples, needles of the KD2 Pro thermal
 18 analyser device were inserted carefully into the prepared sample to measure the thermal conductivity
 19 and volumetric thermal heat capacity. Average values of three measurement readings were taken for
 20 each sample. Fig. 5 presents the thermal conductivity measurements on sand samples as a function
 21 of water saturation. The degree of saturation was determined based on the actual measurement of
 22 the water content at the end of the test. The results clearly show a correlation between increases in
 23 thermal conductivity and increasing water saturation. The thermal conductivity of dry sand was found
 24 to be 0.36 W/m.K. Careful inspection of the data shown in Fig. 5 revealed that the relationship
 25 between thermal conductivity and degree of saturation shows two distinct phases. The first phase is
 26 characterised by a remarkable increase in the thermal conductivity values from 0.36 to 2.6 W/m.K

1 with a slight change in the water saturation while in the second phase, the thermal conductivity values
 2 increased from 2.6 to 3.5 W/m.K over a wide range of water saturation. This could be attributed to
 3 the gradation of the sand used and its water retention properties resulting in a high suction head at
 4 low degrees of water saturation, which in turn caused improved bonding between the particles and
 5 enhanced conductive heat transfer capability. Also shown in Fig. 5 are the measured values for the
 6 volumetric heat capacity of the sand as a function of the degree of water saturation. It is clear that
 7 the volumetric heat capacity (C_v) increased linearly with the degree of saturation which is consistent
 8 with previous observations by Yadav and Saxena, 1973; Ghuman and Lal,1985 and Abu-hamdeh, 2003.

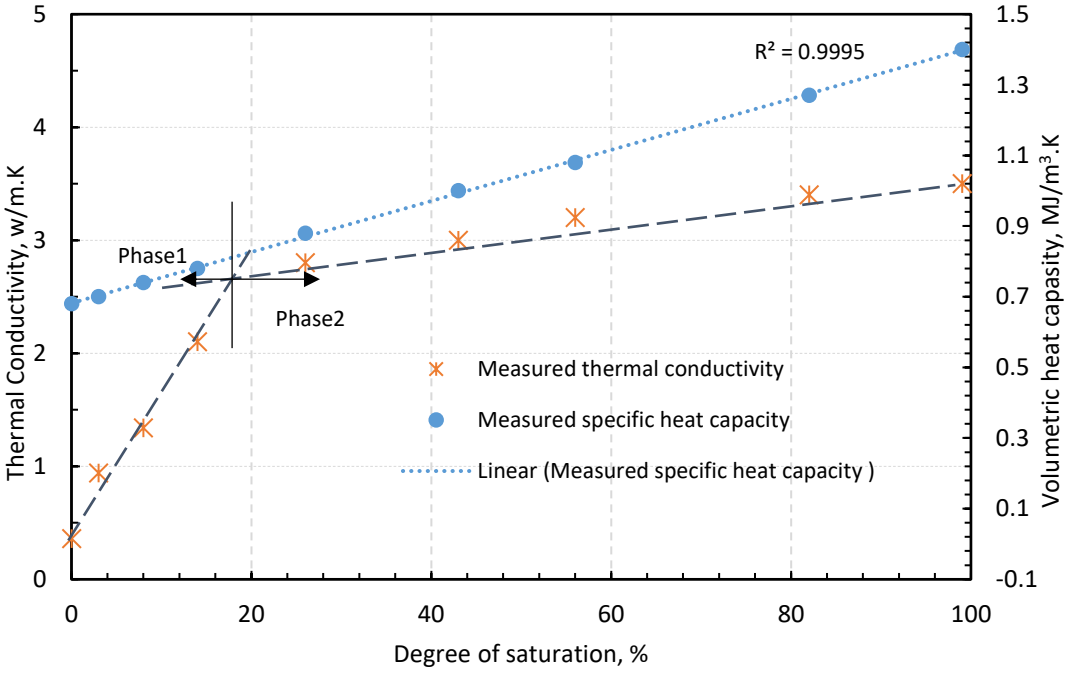


Fig. 5. Measured thermal conductivity of sand as a function the degree of water saturation

3.2 Thermal conductivity, strength and stiffness of concrete

23 The attained results for the thermal conductivity of concrete samples prepared with 0 %, 10 %, 20 %, 24 30 %, 40 % and 50 % graphite (graphTHERM) content of cement weight and tested at room 25 temperature are presented in Table 4. It should be noted that the data presented in Table 4 represents 26 the average value of the thermal conductivity attained from tests on three identical concrete samples

1 whilst batch 1 was carried out as a control test. Consequently, the degree of improvement was
2 determined in comparison to the results attained from the control test. It can be observed that the
3 highest thermal conductivity value was recorded for a concrete made with a graphite content of 50
4 %. The measured thermal conductivity was 3.10 W/m.K which was more than double that obtained
5 on a normal concrete sample (1.44 W/m.K). The enhanced thermal conductivity could fundamentally
6 be attributed to the higher thermal conductivity value of the graphTHERM which was typically 100
7 W/m.K but also to the particle size of graphTHERM, which is , smaller than that of the cement, could
8 have contributed to filling of the tiny voids between the aggregates thereby resulting in an improved
9 packing of particles and a higher density concrete. In other words, replacing the air voids in the
10 concrete with higher thermal conductivity particles could result in a significant increase in the thermal
11 conductivity of concrete (Meng and Khayat, 2016 and Arora et al., 2018). The data plotted in Fig. 6
12 suggest that the relationship for the thermal conductivity of concrete as a function of graphite powder
13 content took the form of an S-shape curve characterised by three distinct regions. With the addition
14 of up to 10.5 % of graphite powder by the weight of cement, a moderate degree of improvement in
15 the thermal conductivity can be observed in region 1. Whereas in region 2, a remarkable degree of
16 improvement in the thermal conductivity of concrete was recorded with the increase in the graphite
17 powder content up to 35.5 %. Any further increase in the graphite content above 35.5 % led to another
18 moderate degree of improvement in the thermal conductivity of concrete. Results reported by
19 Qingwen et al. (2018) suggested that in order to observe a positive change in the value of the thermal
20 conductivity of concrete, more than 15 % of graphite should be added to the concrete. Of note, no
21 optimum value for the graphite content was suggested by the study, nor was the impact on the
22 mechanical behaviour assessed.

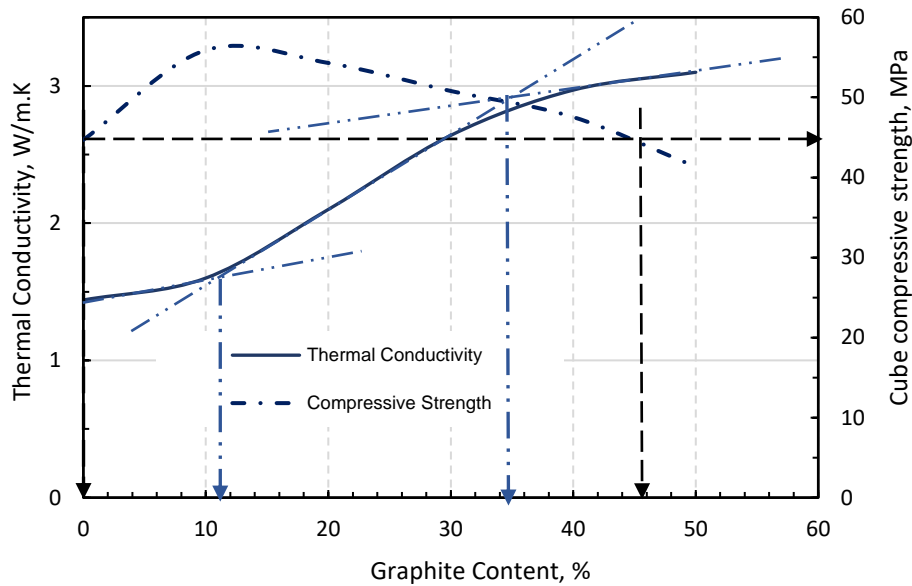
23 Table 4: Thermal conductivity of concrete mixed with different percentages of graphite

Batch number	Graphite Content %	Room Temperature °C	Thermal Conductivity W/m.K	Degree of improvement %
1	Zero	24.4	1.44	-
2	10	24.7	1.60	11
3	20	25.9	2.10	45
4	30	24.6	2.64	83
5	40	24.3	2.97	104
6	50	24.8	3.10	115

1

2 Data for the influence of graphTHERM content on the measured compressive strength of concrete
3 after 28 days of curing were also plotted in Fig. 6. It was observable that the addition of graphTHERM
4 powder to the concrete mix resulted in a considerable degree of improvement in the compressive
5 strength of concrete up to 10 % graphTHERM content. A more than 10% addition of the graphTHERM
6 powder led to a gradual but slight decline in the measured compressive strength. However, the
7 measured compressive strength was still higher than that recorded in the control test on normal
8 concrete with 0 % graphTHERM powder content. The results revealed that adding more than 45 % of
9 graphite powder resulted in achieving a lower strength below that recorded for the normal concrete
10 with zero graphite powder content. Strengthening of concrete by incorporation of graphite powder
11 was previously reported and interpreted by Dimov et al. (2018). Graphite powder would interact with
12 cement in the presence of water to produce Calcium Silicate Hydrate (C-S-H) which is different to that
13 produced in the case of normal concrete and would affect the morphology of the hydration. These
14 changes promote a growth of C-S-H along the graphite particles which enhanced the bond strength of
15 the cement. Results for the microstructure of graphite-concrete taken by X-ray diffraction (XRD)
16 indicated the modification of cement crystals upon graphite incorporation, more specifically to
17 calcium aluminoferrite, calcium carbonate, tri- and di-calcium silicate as well as calcium aluminate
18 (Dimov et al., 2018). The microstructural changes in the crystals at the early stage of hydration are
19 responsible for the strength growth at late stages e.g 28 days.

1 In order for an optimum graphite content to be determined for geo-structural applications, both
 2 compressive strength of concrete and thermal conductivity were taken into consideration. From Fig.
 3 6, it is clear that there is a range for the graphite content which can result in enhancing both thermal
 4 conductivity and concrete compressive strength over those recorded for normal concrete. It was
 5 determined essential that any addition of graphite powder should not reduce the compressive
 6 strength of concrete. The results suggest that addition of 36 % of graphite powder content to concrete
 7 material is effective in terms of enhancing the thermal conductivity by 100 % (top of region 2) whilst
 8 also resulting in a better compressive strength of graphite concrete, which was 10 % higher than that
 9 attained for the control test on normal concrete (0% graphTHERM content).

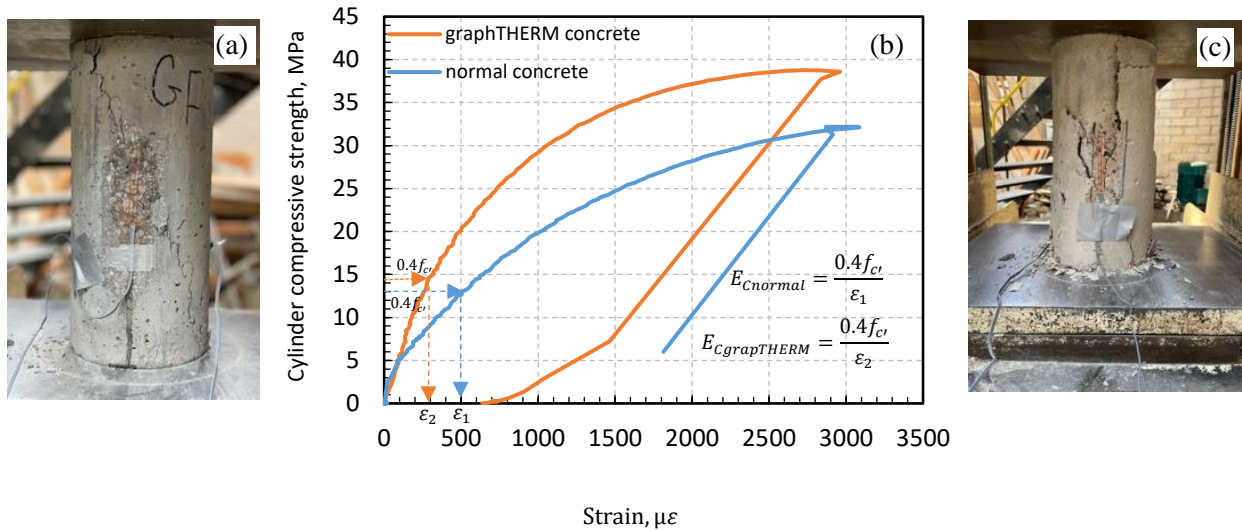


10

11 Fig. 6. Thermal conductivity and cube compressive strength of concrete as a function of the graphite content.
 12 Stiffness of normal concrete and graphTHERM concrete prepared with an optimum value of graphite
 13 powder was measured on cylindrical samples with a diameter of 150 mm and length of 300 mm.
 14 Samples were cured in a water bath for 28 days and air dried for 24 hours prior to testing. Strain
 15 gauges were fastened on the sample surface in the longitudinal direction as shown in Fig. 7a and c.
 16 Fig. 7b shows recorded data for the applied stress and measured strain on samples made from normal
 17 concrete and graphTHERM concrete attained on cylindrical samples. The compressive strength
 18 presented in Fig.7b is therefore the cylindrical compressive strength. The modulus of elasticity (E) was

1 determined from the measured data in accordance with EN 1992-1-2,2004. The results reveal that the
 2 stiffness of the graphTHERM concrete and normal concrete is found to be 32 GPa and 27.8 GPa
 3 respectively. It is clear that the stiffness of graphTHERM concrete is 15 % greater than that measured
 4 for the normal concrete. The increase in stiffness of graphTherm concrete could be attributed to
 5 combining C-S-H which has a Young's modulus E of 23.8 GPa with graphite particles with E value of
 6 2000 GPa (Tanabe et al., 2008 and Dimov et al., 2018). This would lead to a considerable increase in
 7 the elasticity modulus of the graphite-concrete. Moreover, addition of graphite powder assists with
 8 the reduction in the concrete porosity as it extends the size range of microscale dimension of the
 9 particles and increases the packing density for the mix (Sbia et al., 2015 and Arora et al., 2018).

10



11

12

13 Fig. 7. Cylinder compressive strength vs strain for normal concrete and graphTHERM concrete.

14 **3.3 Heat transfer experiments for energy pile**

15 Throughout all tests, the circulating fluid temperature was recorded at the inlet and outlet points of
 16 the HE that was embedded in the model geo-energy pile. The inlet-outlet temperature difference Δt
 17 would indicate the highest amount of heat energy that the pile was able to dissipate into the soil. Fig.
 18 8 presents the temperature difference between inlet and outlet from the four tests and evidently
 19 demonstrates that test W-GP-4 in which the energy pile made of graphite concrete and installed in
 20 partly saturated sand gave the highest temperature difference. On average a difference of about 3 °C
 21 was recorded after reaching steady state conditions in comparison to a measured temperature

1 difference on normal concrete pile in partly saturated sand of 2 °C, indicating a degree of improvement
2 of 50 % while the degree of improvement in temperature difference between inlet and outlet
3 decreased to 31% when the piles were tested in dry soil conditions. These findings provide reliable
4 evidence that the thermal performance of geo-energy pile increased when the graphite concrete was
5 used which could be attributed to the higher thermal conductivity of graphite concrete than that of
6 normal concrete as illustrated in Fig 8.

7 In addition, as illustrated in Fig. 3, the circulating fluid temperature was measured at two more points;
8 points 1 and 2 inside the HE at a distance of 450 mm and 1450 mm from the inlet point respectively.
9 Of note, the total length of pipe within the HE was 1700 mm. Data for the measured temperature, the
10 temperature difference from that measured at the inlet point and the percentage of temperature
11 dissipation at the two points after reaching steady state conditions are presented in Table 5. The data
12 demonstrates that the fluid temperature flowing in the HE reduced by about 20 % and 90 % of the
13 total dissipated temperature at points 1 and 2 respectively. To evaluate the effect of water saturation
14 on the liquid temperature dissipation, the temperature difference $\Delta t_{1-2} = T_1 - T_2$ was determined and
15 presented in Table 5. The results clearly showed for energy piles with normal concrete tests D-NP-1
16 and W-NP-3 that saturating the sand up to mid height of the pile caused a 37 % increase in the
17 temperature difference between points 1 and 2. This could be attributed predominantly to the fact
18 that the soil in the bottom half of the tank was fully saturated with water leading to remarkably higher
19 thermal conductivity and heat capacity. To confirm this observation, measurements for the thermal
20 conductivity and volumetric thermal heat capacity of soil were taken on samples at predetermined
21 heights after the completion of the tests W-NP-3 and W-GP-4. In addition, samples were extracted
22 precisely at the same predetermined heights for determination of water content and density. Fig. 9
23 presents water distribution inside the testing tank which confirms that sand in the bottom half of the
24 tank is fully saturated with water. Of note, there is a significant drop in the degree of saturation in the
25 top 300 mm of the sand reaching an almost dry condition at the surface of the sand. Then, the
26 obtained value of the soil degree of saturation was used in conjunction with Fig.5 to measure the

1 thermal conductivity and heat capacity of the sand along the tank height. Also, presented in Fig. 9, is
 2 the measured thermal conductivity against the degree of saturation. The measurements reveal that
 3 thermal conductivity and heat capacity retained high values in the bottom half of the tank and
 4 decreased gradually towards the sand surface (top of the tank).

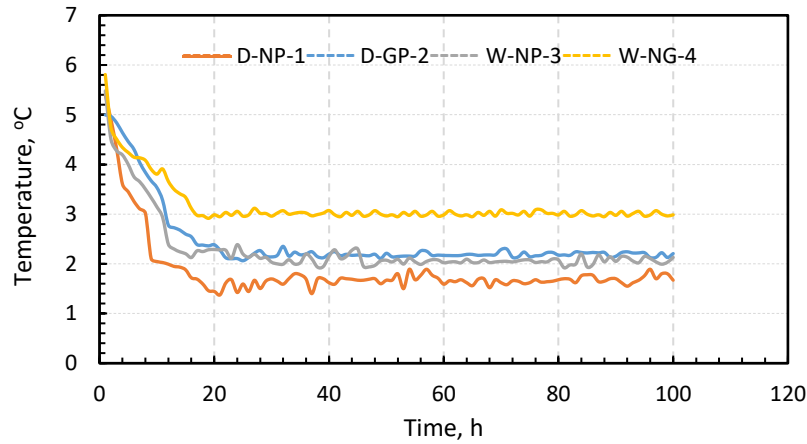


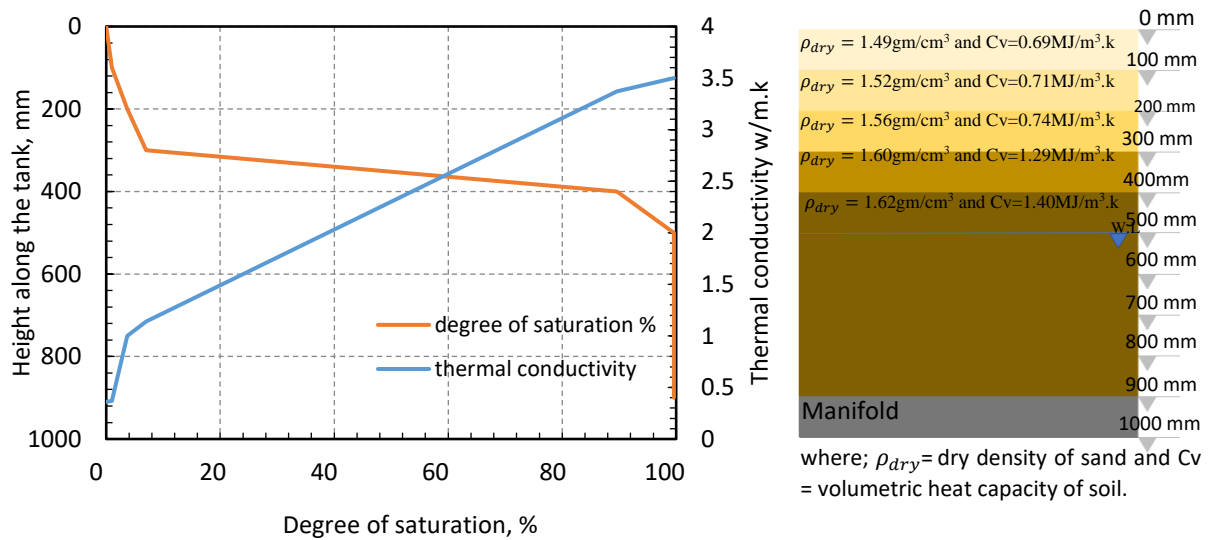
Fig. 8. Measured temperature difference between inlet and outlet

Table 5. Circulating fluid temperature along the heat exchanger

TEST CODE	INLET POINT		POINT 1 (T ₁)				POINT 2 (T ₂)			POINT2 - POINT1	OUTLET POINT		DISSIPATED ENERGY
	T _i	T ₁	Δt ₁	HD	T ₂	Δt ₂	HD	Δt ₁₋₂	T _o	Δt ₃	q		
	°C	°C	°C	%	°C	°C	%	°C	°C	°C	watts		
D-NP-1	52.14	51.76	0.39	23	50.65	1.52	92	1.11	50.49	1.65	113.50		
D-GP-2	52.41	51.97	0.44	20	50.46	1.95	90	1.51	50.25	2.16	148.65		
W-NP-3	52.01	51.6	0.46	22	50.07	1.94	95	1.53	49.96	2.05	141.10		
W-GP-4	52.52	51.75	0.77	25	49.58	2.94	96	2.17	49.45	3.07	211.27		

14 where; T_i = inlet temperature, T₁ = Circulating fluid temperature at 450 mm, T₂ = Circulating fluid temperature at
 15 1450mm, T_o = Outlet temperature, Δt₁ = T_i - T₁, Δt₂ = T_i - T₂, Δt₃ = T_i - T_o, Δt₁₋₂ = T₁ - T₂, HD = percentage of temperature
 16 dissipation, q = dissipated energy.

17



1 Fig. 9. Measured degree of saturation and thermal properties along the experimental tank.

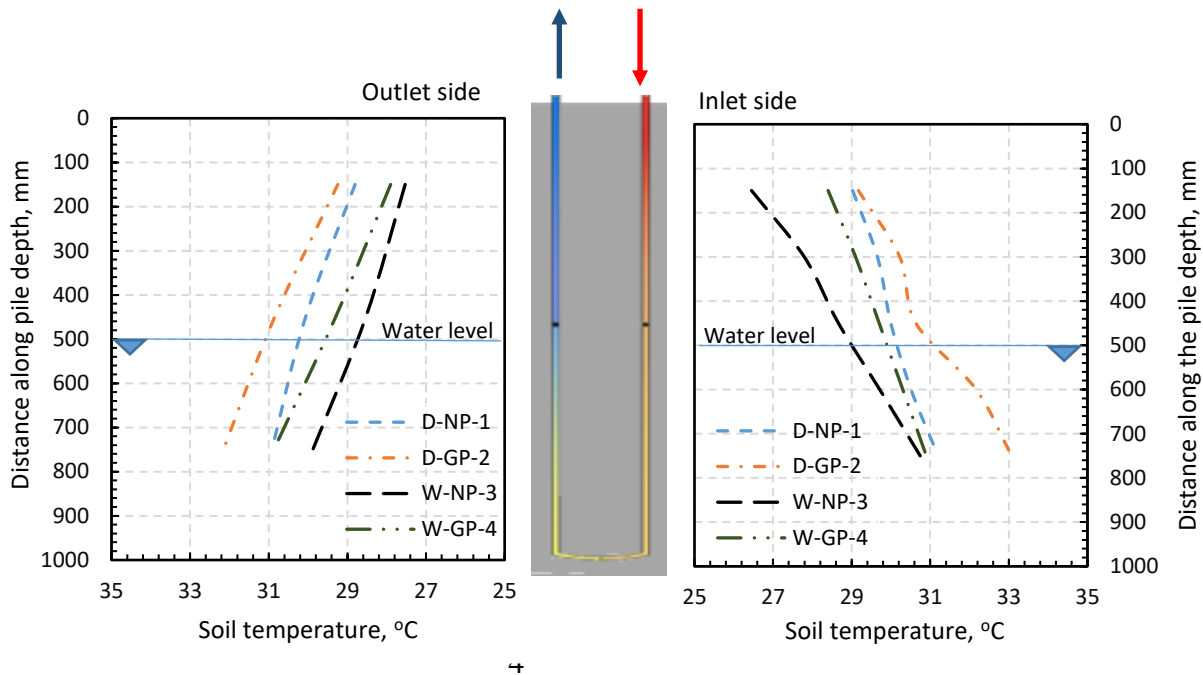
2 Fig. 10 shows the change in the soil temperature measured at five points along the depth of the pile
3 at 150 mm, 300 mm, 450 mm, 600 mm and 750 mm in the inlet side and at three points at 150 mm,
4 450 mm and 750 mm in the outlet side. All measurements were taken at 100 mm away from the pile
5 in both inlet and outlet sides as shown in Fig 3. With the increase in the experimental time, the soil
6 temperature increased until reaching steady state conditions after 20 h from the onset of the test. Fig.
7 10 therefore shows the results of the vertical profile of soil temperature after reaching steady state
8 conditions. The maximum soil temperature recorded at 750 mm for D-GP-2 test is found to be around
9 33 °C which reduced by 2 °C in W-GP-4, recording 31°C. It was evident that the temperature gradient
10 was much steeper at the top half of the pile which suggested that most of the dissipated heat was
11 recorded in the lower soil layers of the tank where the sand has a higher specific heat capacity value
12 due to being saturated. Tests in which geo-energy piles were installed in dry sands showed a higher
13 soil temperature along the vertical profile. Furthermore, the gradient of soil temperature in tests
14 performed on normal and graphite concrete piles installed on partly saturated sand demonstrated a
15 considerable reduction in the soil temperature in comparison to that measured in dry sand. Comparing
16 the vertical temperature profiles recorded on the four geo-energy piles illustrated that the
17 temperature gradient in the adjacent soil was strongly affected by the concrete thermal characteristic.

1 It was obvious that the dissipation of heat from the graphTHERM concrete pile did not cause the soil
2 temperature to increase to the normal concrete pile level despite the fact that it enabled a higher heat
3 dissipation. To calculate the dissipated heat, Equation 2 was used:

$$q = \dot{m}c_p(T_{out} - T_{in}) \quad (2)$$

4 where; q is the thermal energy dissipated into the ground (watts), \dot{m} is the mass flow rate ($\text{kg}\cdot\text{s}^{-1}$), C_p
5 the thermal capacity ($\text{J}\cdot\text{kg}^{-1}\cdot\text{K}^{-1}$) and T_{inlet} and T_{outlet} are the inlet and outlet temperatures
6 respectively. For dry tests, D-NP-1 and D-GP-2, the calculated dissipated heat was about 113.50 watts
7 and 148.6 watts respectively, while for partly saturated soil tests, the dissipated heat was about
8 141.10 watts for W-NP-3 and 211.27 watts for W-GP-4. Fig. 10 also shows that the soil temperature
9 was elevated on both sides of the pile due to dissipation of heat via the HE. Tests D-NP-1 and D-GP-2
10 ~~that were~~ carried out in dry soil conditions, showed higher soil temperature. On the other hand,
11 results from tests W-NP-3 and W-GP-4 indicated that a lower soil temperature was recorded in
12 comparison with those measured for dry soil. This phenomenon could be attributed to the fact that
13 the specific heat capacity is different for dry and saturated sand. Specific heat capacity is defined as
14 the amount of energy to unit increase in the temperature of a unit mass of material. Therefore, it
15 needed more energy to be rejected from the geothermal pile to observe an identical change in
16 temperature in the saturated sand. These results are in consensus with previous work carried out by
17 Mohamed et al. (2015), Kramer (2013) and Bao et al. (2019).

1



5

Fig. 10. Vertical temperature profile of the soil at 100 mm away from the pile

6

The horizontal soil temperature profile at mid-height of the pile (450 mm below the soil surface)

7

measured on both inlet and outlet sides are shown in Fig. 11. As can be seen in Fig.11, due to the high

8

temperature gradient between the pile and the surrounding soil, the soil temperature has increased

9

until reaching the steady state conditions. The maximum increase in the soil temperature from its

10

initial state ($20 \pm 1^\circ\text{C}$) was recorded at $\sim 15^\circ\text{C}$ in tests carried out on dry sand. This could be attributed

11

to its lower heat capacity and thermal conductivity (Kramer, 2013, Faroki, 1986 and Alrtimi et al.,

12

2014). Whereas, when the energy pile was installed in a partly saturated sand, the maximum soil

13

temperature difference was found to be 10°C resulting in a reduction of 33 %. In addition, with the

14

increase in the radial distance from the pile, there was a significant decrease in the soil temperature.

15

The maximum temperature change at 50 mm, 100 mm, 200 mm, 300 mm and 425 mm away from the

16

pile surface were 14.5°C , 10.6°C , 6.50°C , 3.64°C and 1.68°C respectively. Hence, the temperature

17

reached a relatively stable state at approximately 300 mm on both sides, which was as twice as the

18

pile diameter.

19

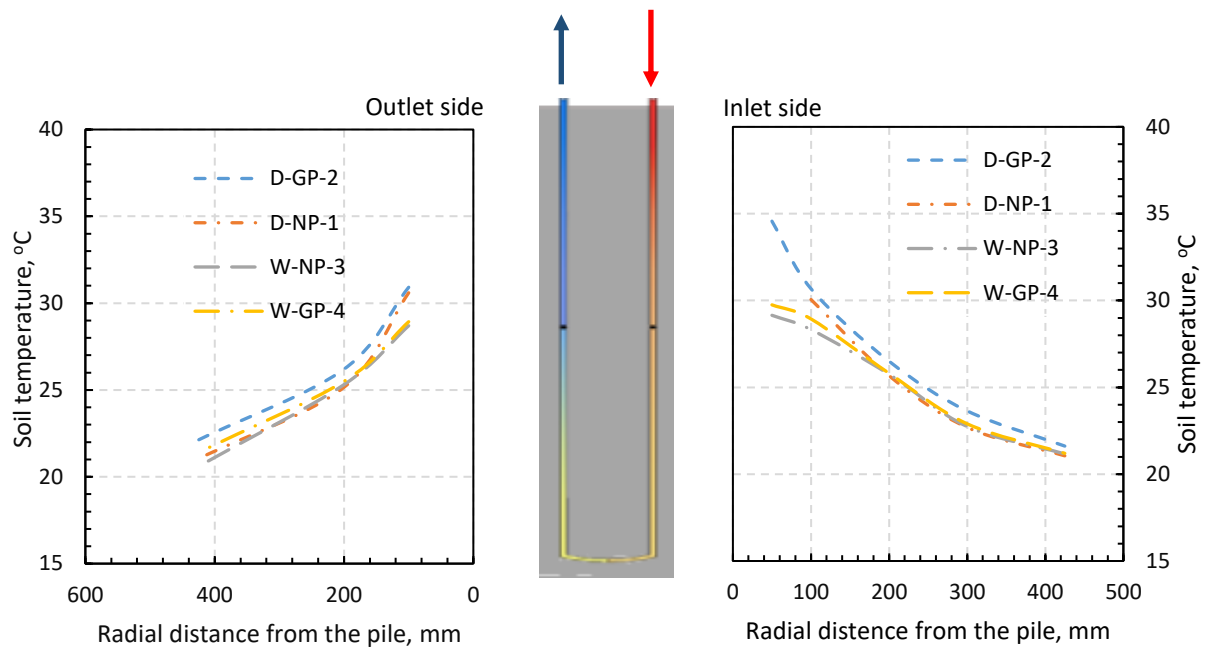


Fig. 11: Soil horizontal temperature profile at mid-height of the pile

Fig. 12 (a and b) showed the lateral earth pressure measured at mid-height of the pile. The lateral pressure cell was placed at the pile-soil interface of the pile in the inlet side. The data were captured from tests on geo-energy piles made from normal concrete and graphTHERM concrete and installed in dry sand and partly saturated sand. The initial values of the lateral earth pressure were approximately 4.8 kPa and 5.79 kPa on piles installed in dry and partly saturated sand beds respectively. The lateral earth pressure was slightly increased by circa 10 Pa after running the experiment for 20 h. This could be attributed to the induced thermal expansion due to heating that in turn led to an increase in the lateral earth pressure at the soil-pile interface. To ascertain the observed behaviour, the thermal strain due to thermal expansion of the pile was calculated in accordance with EN 1992-1-2 as given by Equation 3.

$$\varepsilon_{thermal} = \Delta T * CTE \quad (3)$$

where; CTE is the coefficient of thermal expansion for concrete and ΔT is the temperature difference on concrete which was measured during the test. To accurately calculate the thermal strain, it was crucial to determine the coefficient of thermal expansion. Experiments were conducted in accordance with TI-B 101 (94) on samples of normal concrete and graphTHERM concrete with an optimum percentage of graphTHERM. The coefficient of thermal expansion was found to be $2.002 \times 10^{-6} \text{ } ^\circ\text{C}^{-1}$ and $5.024 \times 10^{-6} \text{ } ^\circ\text{C}^{-1}$ for graphTHERM concrete and normal concrete respectively. Fig. 13 illustrates that the

1 increase in pile temperature led to an increase on the thermal strain. The calculated thermal strain of
2 the normal concrete pile was 45 % higher than that for the graphTHERM concrete pile. This could be
3 attributed to the coefficient of thermal expansion of the normal concrete which was determined
4 experimentally and found to be about 2.5 times greater than that measured for graphTHERM
5 concrete.

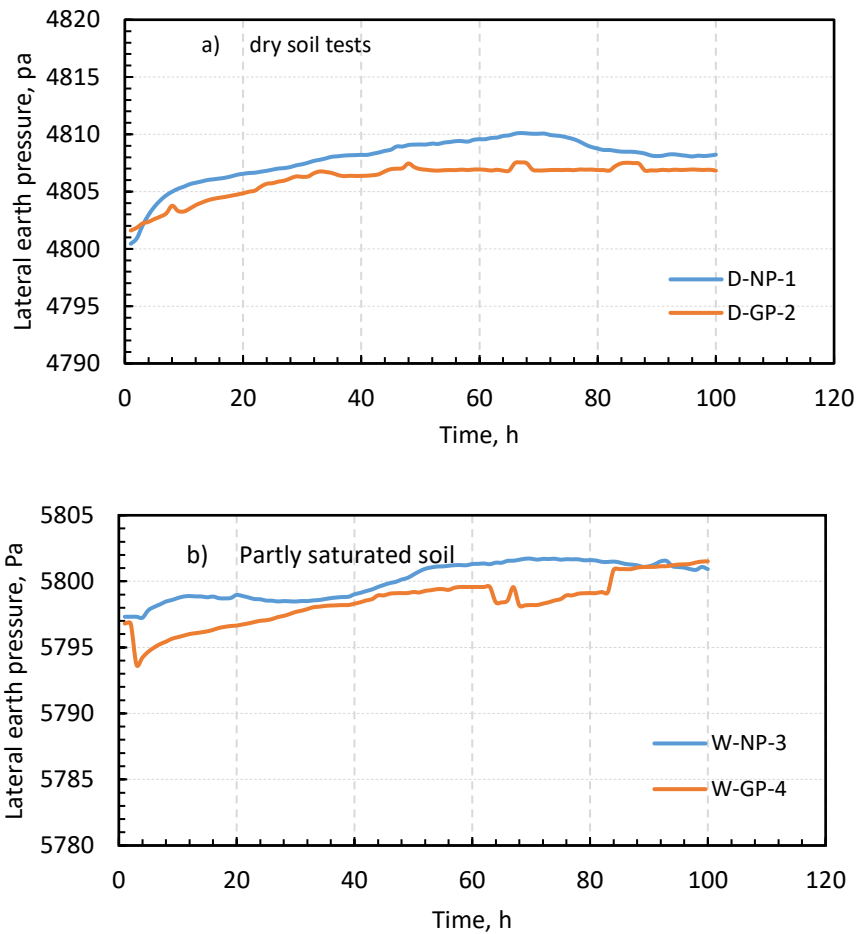


Fig. 12. Lateral earth pressure for a) dry soil tests and b) partly saturated soil tests

1
2
3
4
5
6
7
8
9
10
11
12
13
14
15
16
17
18
19
20
21
22

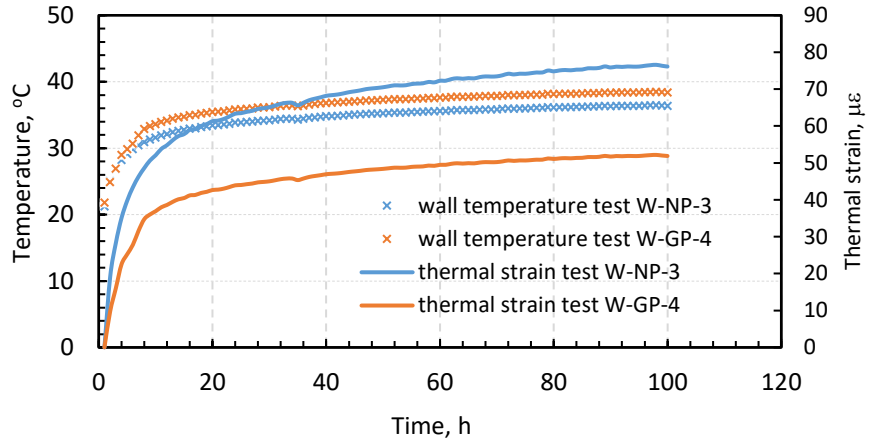


Fig. 13. Pile temperature against thermal strain for W-NP-3 and W-GP-4

3.6 Heat transfer through geo-energy walls

Tests W-NW-1 and W-GW-2 were carried out using geo-energy walls made from normal concrete and thermally enhanced concrete, installed in partly saturated sand. Temperature measurements taken for the circulating fluid were recorded at the inlet and outlet points of the heat exchanger. Fig. 14 presents data for the inlet-outlet temperature difference measured on normal and graphTHERM concrete geo-energy wall. The data evidently demonstrate that the graphTHERM concrete wall (W-GW-2) produced a higher temperature dissipation of 9.67 °C compared with a temperature difference of 6 °C dissipated by the normal concrete wall after reaching steady state conditions. These results illustrate that the thermal performance of geo-energy walls increases by 66 % when graphite concrete was used. This may be attributed to the fact that inclusion of graphite powder in the concrete contributed significantly to fill the tiny voids with highly thermal conductive material resulting in a considerable reduction in the degree of porosity and improvement in its thermal conductivity as suggested by Arora et al. (2018). This led to the dissipation of more heat to adjacent soils which in turn enhanced the performance of heat pumps.

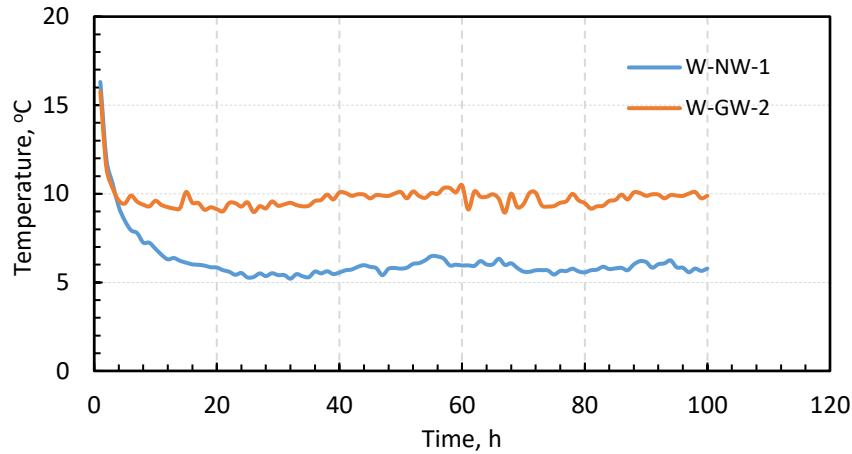


Fig. 14. Temperature difference (inlet-outlet)

1
2
3
4
5
6
7
8
9
10

In addition to measuring inlet and outlet temperatures, temperature measurements were taken at 4 more points: P1, P2, P3 and P4 at a distance of 900 mm, 2950 mm, 4950 mm and 6950 mm along the 9900mm long heat exchanger (see Fig. 4c). Fig. 15 (a and b) shows data for the temperature measurements at the six points from tests on geo-energy walls made from normal concrete and thermally enhanced concrete respectively. The results show that the temperature drop from that recorded at the inlet T_i was almost the same in both tests W-NW-1 and W-GW-2. The measured fluid temperature was reduced by about 11 % at P_1 and 70% at P_4 as illustrated in Table 6. The fluid temperature gradient along the embedded heat exchanger was considered to decline uniformly.

1

Table 6: Circulating fluid temperature along the heat exchanger

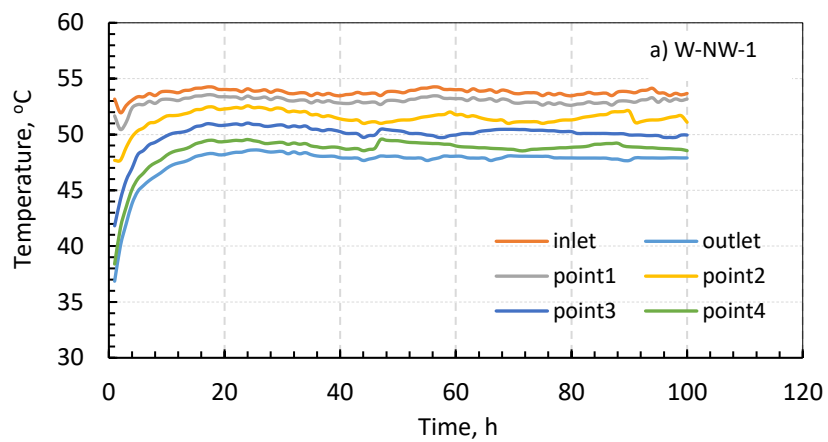
TEST CODE	INLET POINT		POINT 1		POINT 4			OUTLET POINT		DISSIPATED ENERGY
	T_i	T_1	Δt_1	HD	T_4	Δt_4	HD	T_o	Δt_6	q
	°C	°C	°C	%	°C	°C	%	°C	°C	watts
W-NW-1	53.81	53.05	0.76	13	50.29	3.52	61	47.98	5.82	400.53
W-GW-2	52.35	51.45	0.90	10	46.16	6.19	67	42.67	9.67	665.53

2

where; T_i = inlet temperature, T_1 = liquid temperature at 900 mm, T_4 = liquid temperature at 6950mm, T_o =outlet temperature, $\Delta t_1=T_i-T_1$, $\Delta t_4=T_i-T_4$, $\Delta t_6=T_i-T_o$, HD = percentage of temperature dissipation.

3

4



5

6

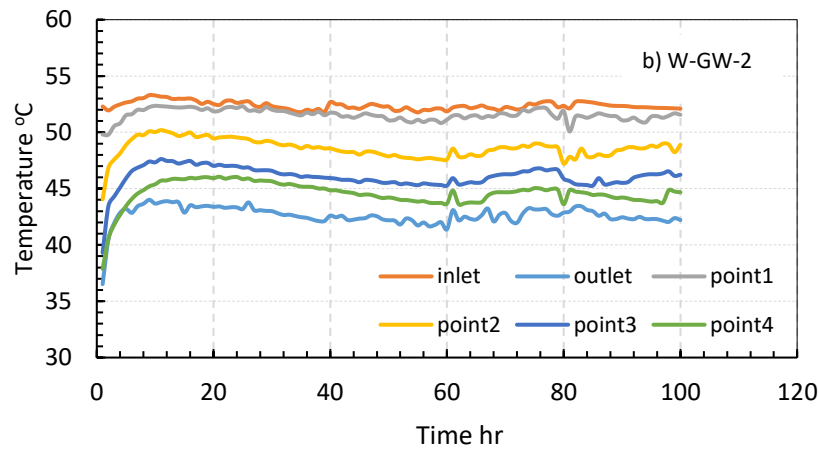
7

8

9

10

11



12

13

14

15

16

17

Fig. 15. Circulating fluid temperature along the heat exchanger a) normal concrete wall and

18

b) graphTHERM concrete wall

19

The vertical soil temperature profiles measured at two vertical sections V1 and V2, located at 100 mm and 300 mm away from the experimented energy wall as shown in Fig.3. Measurements of temperature along V1 were taken at a depth of 150 mm, 300 mm, 450 mm, 600 mm, and 750 mm, while those along V2 were recorded at 150 mm, 450 mm and 750 mm. Data for the temperature

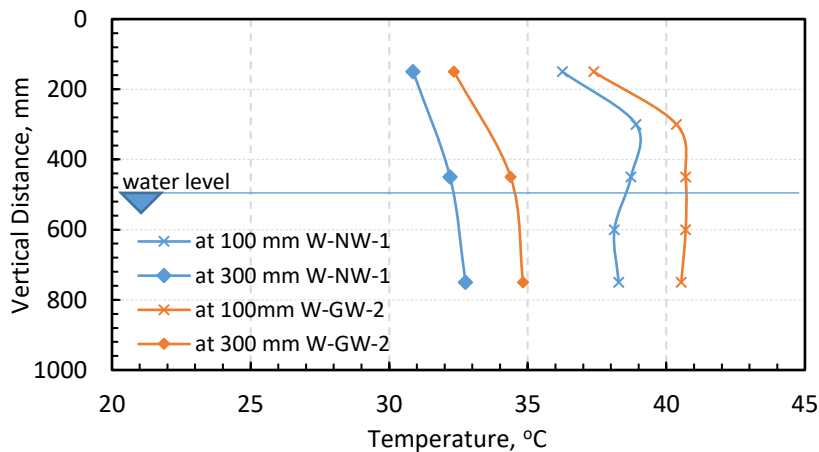
20

21

22

23

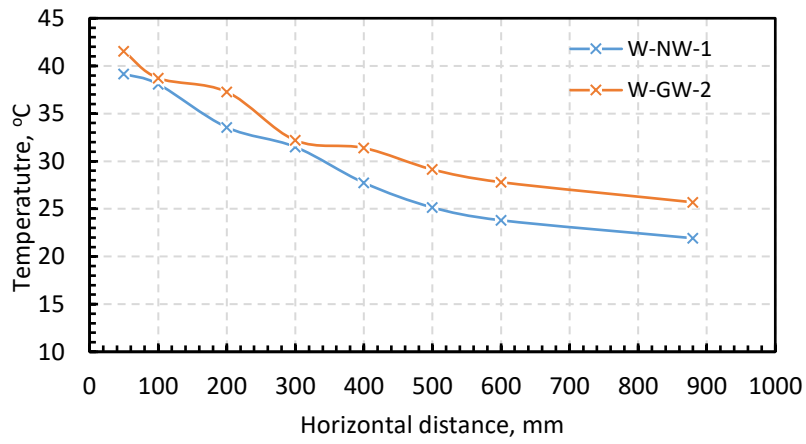
1 measurements taken at two vertical sections namely V1 and V2 were plotted in Fig. 16 after reaching
 2 steady state conditions. The data show clearly that the soil temperatures at section V1 were
 3 significantly higher than those measured further away at section V2. Furthermore, it can be observed
 4 that the influence of the graphTHERM concrete energy wall (W-GW-2) on the soil temperature was
 5 significant in comparison with that produced by the geo-energy wall made from normal concrete (W-
 6 NW-1). This reflects principally the ability of each type of wall to dissipate heat into the surrounding
 7 soil. Equation 2 was used to calculate the dissipated heat from the energy walls and found that, W-
 8 GW-2 dissipated heat of about 665.53 watts, while W-NW-1 dissipated 400.53 watts. Hence, the
 9 graphite concrete wall dissipated more than 50 % heat to adjacent soils which would result in a higher
 10 temperature variation in the surrounding soils.



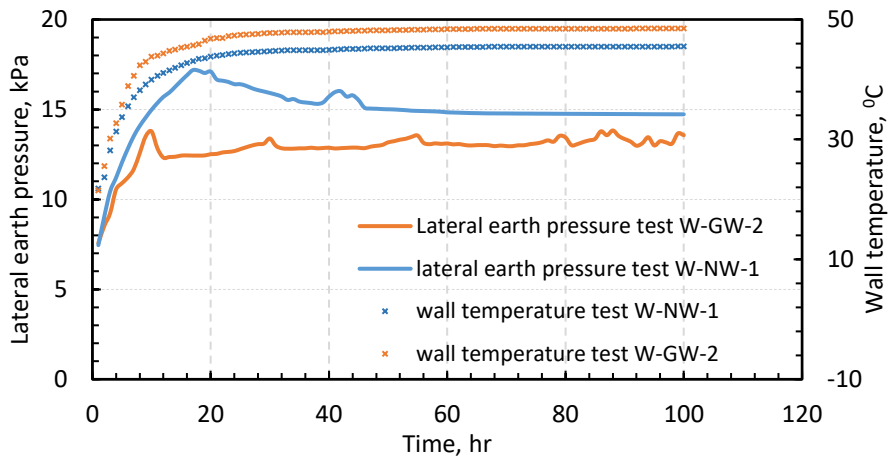
17 Fig. 16. Vertical soil temperature profile for W-NW-1 and W-GW-2

19 The horizontal soil temperature profile measured at mid-height of the wall is presented in Fig. 17. Soil
 20 temperature was measured at 50 mm, 100 mm, 200 mm, 300 mm, 400 mm, 500 mm, 600 mm and
 21 880 mm away from the wall. It was observed that an interference region between the wall and soil
 22 can be considered as the most affected region in the experimental tank. From the results of the two
 23 tests, a soil-wall interference region was identified to be around 400 mm. Initially, the soil temperature
 24 was 21°C which was increased intensely to reach almost 41.5 °C at 50 mm away from the wall after
 25 reaching steady state conditions for graphTHERM concrete wall. For the same measurement point the
 26 temperature gradient reduced by 2 °C to be almost 38 °C when the normal concrete was used. The

1 figure also indicated the steady state soil temperature reduced when increasing the horizontal
 2 distance from the wall.



11 Fig. 17. Horizontal soil temperature profile for W-NW-1 and W-GW-2



24 Fig. 18. Lateral earth pressure on walls made out of normal concrete and graphite concrete

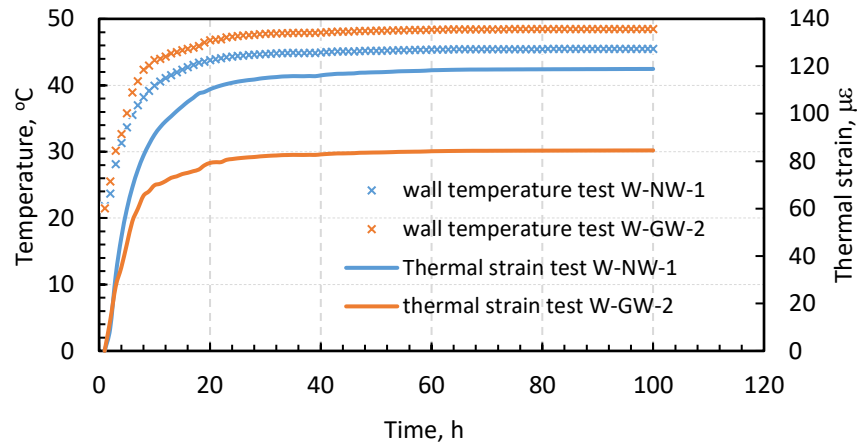


Fig. 19. Wall temperature and thermal strain versus time

1
2
3
4
5
6
7
8
9
10
11
12
13
14
15
16
17
18
19
20

Fig. 18 shows the measured lateral pressure at mid-height of the wall in case of a normal concrete and graphite concrete wall. The experimental results are evidence that heating the geo-energy wall induced thermal expansion which in turn increased the lateral earth pressure applied on the wall surface. In other words, the lateral earth pressure increased with the increase in wall temperature irrespective of the concrete type until reaching almost a constant value after running the tests for 40 hours. The maximum lateral earth pressure was double that measured at the onset of the experiment. According to Dong et al. (2019), the increase in lateral earth pressure could have a significant contribution to the vertical stress within a wall. In the case of the graphTHERM concrete wall, the excess lateral earth pressure was 8 kPa to 13.8 kPa whilst for normal concrete wall, 8 kPa to 15 kPa. The results suggest that the graphTHERM concrete wall produced 8% lower lateral earth pressure than that measured on a normal concrete wall. To explain this behaviour, Equation 3 was utilised to determine the thermal strain for both walls as a function of temperature. Data for the thermal strain were presented in Fig. 19 and demonstrate that when the temperature of the wall increased, the correspondingly strain increased. For normal concrete wall the maximum thermal strain was founded to be 119 $\mu\epsilon$ while for the grapTHERM concrete wall, the maximum thermal strain was reduced by 41% to 84 $\mu\epsilon$. This suggested that the Coefficient of thermal expansion for graphTHERM concrete is 2.5 times less than that measured for the normal concrete. In contrast with the pile, the wall generated a higher lateral earth pressure which could be attributed to the relative volume of concrete used for

1 the construction of pile and wall. So, the pile, when subjected to thermal load, would slightly expand,
2 but due to the cylindrical shape of the pile, adjacent sand would arch around it partially absorbing the
3 effect of thermal expansion. Whereas, in case of geo-energy walls, the lateral expansion is greater
4 than that observed on piles and the whole wall would push the sand unidirectionally, thus producing
5 a higher lateral earth pressure. One should note that it is essential that further investigations are
6 carried out to evaluate the effect of graphTHERM concrete on the thermally induced elongation for
7 geo-energy piles and walls and the thermally induced bending for the geo-energy wall to be in line
8 with the recent studies on concrete geo-energy structures by Nicholison et al. (2014); Mimouni and
9 Laloui (2015); Loria and Laloui (2015); Pagol et al. (2018); Dong et al. (2019); Loveridge et al. (2019);
10 Ravera et al. (2020); Loria (2020); Shao et al. (2021) and Sailer et al. (2021).

11

12 **4. Conclusions**

13 A comprehensive experimental investigation was carried out to assess the influence of using thermally
14 enhanced concrete in the construction of two geo-energy structure applications e.g. energy piles and
15 energy diaphragm walls. Based on the experimental results, the following conclusions could be drawn
16 out;

- 17 • The thermal conductivity of graphite-concrete was significantly improved in comparison to
18 that obtained for normal concrete under the same environmental temperature. An
19 improvement of about 11 %, 45 %, 83 %, 100 % and 115 % was recorded when 10 %, 20 %,
20 30 %, 40 % and 50 % of graphTHERM powder was added to the concrete respectively.
- 21 • Considerable improvements in the compressive strength of concrete was achieved when
22 graphTHERM powder was added to concrete. The peak for the compressive strength of
23 graphite concrete was recorded with the addition of 10 % graphite powder. Adding more than
24 45 % of graphite powder to the concrete resulted in achieving a compressive strength that
25 was lower than that of normal concrete.

- 1 • The results suggested that adding 36 % of graphite powder to the concrete enhanced the
2 thermal conductivity by 100 % in addition to achieving 10 % higher concrete compressive
3 strength.
- 4 • The thermal performance of energy pile was remarkably improved by incorporating
5 graphTHERM into concrete whether placed in dry or partly saturated sand. The degree of
6 improvement was found to be 31 % and 50 % when the geo-energy pile was installed in dry
7 and partly saturated sand respectively.
- 8 • The thermal efficiency of geo-energy wall diaphragms was increased by 66% when
9 graphTHERM was added to the concrete.
- 10 • The stiffness of the graphTHERM concrete was higher by 15 % more than that measured for
11 normal concrete.
- 12 • The coefficient of thermal expansion of graphTHERM concrete was found to be 2.5 times less
13 than measured for normal concrete. Therefore, the graphTHERM concrete geo-energy
14 structures would experience less thermal expansion which in turn could lead to less lateral
15 earth pressure.

16

17 **References**

- 18 [1] Thomas, H. R. & Rees, S. W. (2009). *Geotechnique* 59, No. 4, 365–375 [doi:
19 10.1680/geot.2008.59.4.365]
- 20 [2] Kovačević, M.S., Bačić, M. and Arapov, I. (2012) Prospects of underground engineering in the use
21 of shallow energy. *Građevinar*, 64 (12), 1019-1028.
- 22 [3] Suryatriyastuti, M.E., Mroueh, H. and Burlon, S. (2012). Un-
23 derstanding the temperature-induced
24 mechanical behaviour of e- nergy pile foundations. *Renewable and Sustainable Energy Re-
views*, 16, 3344-3354.
- 25 [4] Brandl, H. (2006). Energy foundations and other thermo-active ground
26 structures. *Géotechnique*, 56(2), 81-122.
- 27 [5] Laloui and Di Donna A (2013) *Energy Geostructures: Innovation in Underground Engineering*. ISTE
28 Ltd, London, UK and John Wiley & Sons Inc, Hoboken, NJ, USA. Book
- 29 [6] Faizal, M., Bouazza, A., & Singh, R. M. (2016). Heat transfer enhancement of geothermal energy
30 piles. *Renewable and Sustainable Energy Reviews*, 57, 16-33.
- 31 [7] Cecinato F, Loveridge FA. 2015. Influences on the thermal efficiency of energy piles. *Energy*. 1021-
32 1033 **82**

- 1 [8] Kwag, B. C., & Krarti, M. (2013). Performance of thermoactive foundations for commercial
2 buildings. *Journal of Solar Energy Engineering*, 135(4), 040907.
- 3 [9] Kaltreider, C., Krarti, M., & McCartney, J. (2015). Heat transfer analysis of thermo-active
4 foundations. *Energy and Buildings*, 86, 492-501.
- 5 [10] Loveridge, F., & Powrie, W. (2014). 2D thermal resistance of pile heat
6 exchangers. *Geothermics*, 50, 122-135.
- 7 [11] Y. Li, J. Mao, S. Geng, X. Han, H. Zhang, Evaluation of thermal short-circuiting and influence on
8 thermal response test for borehole heat exchanger, *Geothermics* 50 (2014) 136–
- 9 [12] Gashti, E. H. N., Uotinen, V. M., & Kujala, K. (2014). Numerical modelling of thermal regimes in
10 steel energy pile foundations: A case study. *Energy and buildings*, 69, 165-174.
- 11 [13] Jalaluddin., Miyara, A., Tsubaki, K., Inoue, S., & Yoshida, K. (2011). Experimental study of several
12 types of ground heat exchanger using a steel pile foundation. *Renewable Energy*, 36(2), 764-771.
- 13 [14] Zarrella, A., De Carli, M., & Galgaro, A. (2013). Thermal performance of two types of energy
14 foundation pile: helical pipe and triple U-tube. *Applied Thermal Engineering*, 61(2), 301-310.
- 15 [15] Lyu, W., Pu, H., Xiao, H., Hu, D., & Ma, Q. Thermal performance of energy pile with deeply
16 penetrating 1-U-shape heat exchanger. *Geothermics*, 91, 102023.
- 17 [16] Das, S. K., Choi, S. U., & Patel, H. E. (2006). Heat transfer in nanofluids—a review. *Heat transfer*
18 *engineering*, 27(10), 3-19.
- 19 [17] Ghozatloo, A., Rashidi, A., & Shariaty-Niassar, M. (2014). Convective heat transfer enhancement
20 of graphene nanofluids in shell and tube heat exchanger. *Experimental Thermal and Fluid Science*, 53,
21 136-141.
- 22 [18] Godson, L., Deepak, K., Enoch, C., Jefferson, B., & Raja, B. (2014). Heat transfer characteristics of
23 silver/water nanofluids in a shell and tube heat exchanger. *Archives of Civil and Mechanical*
24 *Engineering*, 14(3), 489-496.
- 25 [19] Noorollahi, Y., Saeidi, R., Mohammadi, M., Amiri, A., & Hosseinzadeh, M. (2018). The effects of
26 ground heat exchanger parameters changes on geothermal heat pump performance—a review.
27 *Applied Thermal Engineering*, 129, 1645-1658.
- 28 [20] S. Selamat, A. Miyara, K. Kariya, Numerical study of horizontal ground heat exchangers for design
29 optimization, *Renew. Energy* 95 (2016) 561–573.
- 30 [21] J. Raymond et al., Designing coaxial ground heat exchangers with a thermally enhanced outer
31 pipe, *Geothermal Energy* 3 (1) (2015) 7.
- 32 [22] S.-J. Cao, X.-R. Kong, Y. Deng, W. Zhang, L. Yang, Z.-P. Ye, Investigation on the thermal
33 performance of steel heat exchanger for ground source heat pump systems using full-scale
34 experiments and numerical simulations, *Appl. Therm. Eng.* 115 (2016) 91–98.
- 35 [23] Dorrian, D., & Mumm, S. M. (2011). *U.S. Patent Application No. 12/835,404*.
- 36 [24] Ye, C. M., Shentu, B. Q., & Weng, Z. X. (2006). Thermal conductivity of high density polyethylene
37 filled with graphite. *Journal of Applied Polymer Science*, 101(6), 3806-3810.
- 38 [25] Kumar, S., & Murugesan, K. (2020). Optimization of geothermal interaction of a double U-tube
39 borehole heat exchanger for space heating and cooling applications using Taguchi method and utility
40 concept. *Geothermics*, 83, 101723.
- 41 [26] Li, Q., Chen, L., Ma, H. and Huang, C.H., 2018. Enhanced Heat Transfer Characteristics of Graphite
42 Concrete and Its Application in Energy Piles. *Advances in Materials Science and Engineering*, 2018.
- 43 [27] Guo, C., Zhu, J., Zhou, W., & Chen, W. (2010). Fabrication and thermal properties of a new heat
44 storage concrete material. *Journal of Wuhan University of Technology-Mater. Sci. Ed.*, 25(4), 628-630.

- 1 [28] Kong, L. P., Qiao, L., Xiao, Y. Y., & Li, Q. W. (2019). A study on heat transfer characteristics and
2 pile group influence of enhanced heat transfer energy piles. *Journal of Building Engineering*, 24,
3 100768.
- 4 [29] Bao, X., Li, Y., Feng, T., Cui, H. and Chen, X., (Bao, Li et al. 2019)2019. Investigation on thermo-
5 mechanical behavior of reinforced concrete energy pile with large cross-section in saturated sandy
6 soil by model experiments. *Underground Space*.
- 7 [30] Kurten, S., Mottaghy, D. & Ziegler, M., 2015. Design of plane energy geostructures based on
8 laboratory test and numerical modelling. *Energy and Buildings*, 107, pp.434–444.
- 9 [31] Di Donna, A., 2016. Energy walls for an underground car park. In 25th European Young
10 Geotechnical Engineering conference. 21-24 June 2016, Sibiu, Romania.
- 11 [32] Sterpi, A. Coletto, L. Mauri, Investigation on the behaviour of a thermo-activediaphragm wall by
12 thermo-mechanical analyses, *Geomech. Eng. Environ.* 9 (2017)1–20
- 13 [33] Bourne-Webb, P. J., Freitas, T. B., & da Costa Gonçalves, R. A. (2016). Thermal and mechanical
14 aspects of the response of embedded retaining walls used as shallow geothermal heat
15 exchangers. *Energy and Buildings*, 125, 130-141.
- 16 [34] Dong, S., Li, X., Tang, A. M., Pereira, J. M., Nguyen, V. T., Che, P., & Xiong, Z. (2019). Thermo-
17 mechanical behavior of energy diaphragm wall: Physical and numerical modelling. *Applied Thermal*
18 *Engineering*, 146, 243-251.
- 19 [35] Di Donna A, Cecinato F, Loveridge F, Barla M. 2017. Energy performance of diaphragm walls used
20 as heat exchangers. *Proceedings of the Institution of Civil Engineers - Geotechnical Engineering*. 232-
21 245 170.3
- 22 [36] TI-B 101 (94), 1994. Testing and Sampling Method Concrete: Thermal Expansion Coefficient.
23 Danish Technological Institute, Denmark.
- 24 [37] EN 1992-1-2, 2004. *Eurocode 2: Design of Concrete Structures - Part 1-2*. 1st ed. Brussels: BSI.
- 25 [38] BSI, 2001. BS EN 12664:2001 Thermal performance of building materials and products. London:
26 BSI.
- 27 [39] Yadav, M. R., & Saxena, G. S. (1973). Effect of compaction and moisture content on specific heat
28 and thermal capacity of soils. *Journal of the Indian Society of Soil Science*, 21(2), 129-132.
- 29 [40] Ghuman, B. S., & Lal, R. (1985). Thermal conductivity, thermal diffusivity, and thermal capacity
30 of some Nigerian soils. *Soil Science*, 139(1), 74-80.
- 31
- 32 [41] Abu-Hamdeh, N. H. (2003). Thermal properties of soils as affected by density and water content.
33 *Biosystems engineering*, 86(1), 97-102.
- 34 [42] Arora, A., Aguayo, M., Hansen, H., Castro, C., Federspiel, E., Mobasher, B., & Neithalath, N.
35 (2018). Microstructural packing-and rheology-based binder selection and characterization for Ultra-
36 high Performance Concrete (UHPC). *Cement and Concrete Research*, 103, 179-190.
- 37 [43] Meng, W., & Khayat, K. H. (2016). Mechanical properties of ultra-high-performance concrete
38 enhanced with graphite nanoplatelets and carbon nanofibers. *Composites Part B: Engineering*, 107,
39 113-122.
- 40 [44]. Dimov, D., Amit, I., Gorrie, O., Barnes, M. D., Townsend, N. J., Neves, A. I., ... & Craciun, M. F.
41 (2018). Ultrahigh performance nanoengineered graphene–concrete composites for multifunctional
42 applications. *Advanced Functional Materials*, 28(23), 1705183.
- 43 [45] Tanabe, T.A., Sakata, K., Mihashi, H., Sato, R., Maekawa, K. and Nakamura, H. eds., 2008. *Creep,*
44 *Shrinkage and Durability Mechanics of Concrete and Concrete Structures, Two Volume Set:*
45 *Proceedings of the CONCREEP 8 conference held in Ise-Shima, Japan, 30 September-2 October*
46 *2008* (Vol. 1). CRC Press.

- 1 [46] Sbia, L. A., A. Peyvandi, P. Soroushian, A. M. Balachandra, and K. Sobolev. 2015. "Evaluation of
2 Modified- Graphite Nanomaterials in Concrete Nanocomposite Based on Packing Density Principles."
3 *Construction and Building Materials*, no. 76: 413–422
- 4 [47] Mohamed, M., El Kezza, O., Abdel-Aal, M., Schellart, A., & Tait, S. (2015). Effects of coolant flow
5 rate, groundwater table fluctuations and infiltration of rainwater on the efficiency of heat recovery
6 from near surface soil layers. *Geothermics*, 53, 171-182.
- 7 [48] Kramer, C. A., MSc in civil engineering (2013). An experimental investigation on performance of
8 a model geothermal pile in sand. The Pennsylvania State University
- 9 [49] Faroki, O. T. (1986). Thermal Properties of Soils "; Series on Rock and Soil Mechanics Vol. 11. *Trans*
10 *Tech Publications*.
- 11 [50] Alrtimi, A., Rouainia, M., & Manning, D. A. C. (2014). An improved steady-state apparatus for
12 measuring thermal conductivity of soils. *International Journal of Heat and Mass Transfer*, 72, 630-636.
- 13 [51] Mimouni, T., & Laloui, L. (2015). Behaviour of a group of energy piles. *Canadian Geotechnical*
14 *Journal*, 52(12), 1913-1929.
- 15 [52] Loria, A. F. R., & Laloui, L. (2016). The interaction factor method for energy pile
16 groups. *Computers and Geotechnics*, 80, 121-137.
- 17 [53] Loria, A. F. R., & Laloui, L. (2017). Displacement interaction among energy piles bearing on stiff
18 soil strata. *Computers and Geotechnics*, 90, 144-154.
- 19 [55] Pagola, M. A., Madsen, S., Jensen, R. L., & Poulsen, S. E. (2018). Thermo-mechanical aspects of
20 pile heat exchangers: background and literature review.
- 21 [56] Ravera, E., Sutman, M., & Laloui, L. (2020). Load transfer approach for the geotechnical analysis
22 of energy piles in a group with slab. In *E3S Web of Conferences* (Vol. 205, p. 05008). EDP Sciences.
- 23 [57] Loria, A. F. R. (2020). Energy geostructures: Theory and application. In *E3S Web of*
24 *Conferences* (Vol. 205, p. 01004). EDP Sciences.
- 25 [58] Shao, D., Jiang, G., Zong, C., Xing, Y., Zheng, Z., & Lv, S. (2021). Global sensitivity analysis of
26 behavior of energy pile under thermo-mechanical loads. *Soils and Foundations*, 61(2), 283-302.
- 27 [59] Loveridge, F., McCartney, J. S., Narsilio, G. A., & Sanchez, M. (2020). Energy geostructures: a
28 review of analysis approaches, in situ testing and model scale experiments. *Geomechanics for Energy*
29 *and the Environment*, 22, 100173.
- 30 [60] Nicholson, D. P., Chen, Q., de Silva, M., Winter, A., & Winterling, R. (2014, June). The design of
31 thermal tunnel energy segments for Crossrail, UK. In *Proceedings of the Institution of Civil Engineers-*
32 *Engineering Sustainability* (Vol. 167, No. 3, pp. 118-134). Thomas Telford Ltd.
- 33 [61] Sailer, E., Taborda, D. M., Zdravković, L., Potts, D. M., & Cui, W. (2021). Thermo-hydro-
34 mechanical interactions in porous media: Implications on thermo-active retaining walls. *Computers*
35 *and Geotechnics*, 135, 104121.

36